Plasticity and thermally-induced recovery in polycarbonate

Mohammed Nadhir D. Cherief, Fahmi Zairi, Ning Ding, Jean-Michel Gloaguen, Moussa Naït-Abdelaziz, Mohamed Benguediab

Version of Record: https://www.sciencedirect.com/science/article/pii/S0167663620305573
Manuscript_89541fbf681d3765a074bdb1fb0fb8db

Plasticity and thermally-induced recovery in polycarbonate

Mohammed Nadhir D. Cherief[a], Fahmi Zaïri[b*], Ning Ding[c], Jean-Michel Gloaguen[d], Moussa Naït-Abdelaziz[e], Mohamed Benguediab[a]

[a]Djillali Liabes University, Laboratoire de Matériaux et Systèmes Réactifs, 22000 Sidi Bel-Abbes, Algeria
[b]Lille University, Civil Engineering and geo-Environmental Laboratory (ULR 4515 LGCgE), 59000 Lille, France
[c]Qilu University of Technology (Shandong Academy of Sciences), Engineering Research Center of Failure Analysis and Safety Assessment, Shandong Analysis and Test Center, 250014 Jinan, China
[d]Lille University, Unité Matériaux Et Transformations (UMR 8207 UMET), 59000 Lille, France
[e]Lille University, Unité de Mécanique de Lille (EA 7572 UML), 59000 Lille, France

*Corresponding author.
E-mail address: fahmi.zairi@polytech-lille.fr

Abstract
In the present paper, we present an approach combining physically-based constitutive modeling and experiments to study the thermo-mechanical response of amorphous thermoplastics whose final objective is the prediction of the thermally-induced strain recovery. The underlying thermo-mechanical mechanisms are described by elastoviscoplastic-viscohyperelastic constitutive relations allowing to account for the variation with temperature of the inter and intramolecular barriers to deformation and their abrupt change when the temperature traverses the glass transition. The model fit shows a good agreement with experimental observations on polycarbonate in terms of temperature and strain-rate dependent stress-strain response. The material kinetics with temperature is designed and introduced into the model to predict the thermally-activated strain recovery process during heating. In our approach, the intramolecular resistance of the entangled molecular chain network orientation/relaxation is used as the driving stress that continuously activates the strain recovery process during zero-stress creep above glass transition. The model predictions are shown under zero-stress creep recovery for different previous loading histories in terms of strain-rate and strain-level. The simulated results are in satisfactory agreement with experimental observations at different heating temperatures showing the relevance of the proposed approach.

Keywords: Amorphous thermoplastics; Thermally-induced recovery; Viscoplasticity; Viscohyperelasticity.

1. Introduction
Plasticity is a common term to designate the propensity of a material to undergo unrecoverable alteration of the microstructure by the action of a mechanical loading: the material remains deformed after the mechanical loading is removed. Although amorphous polymers exhibit what appears as a plastic deformation well described now in the literature, paradoxically, the "apparent" plasticity may be regarded as a frozen process only at the loading time-scale since it may be fully or partially recovered in response to a suitable stimulus such a temperature change. The purpose of this contribution is to come back to this

subject by studying the thermally-induced recovery of the apparent plasticity, in the specific case of polycarbonate, by an approach combining constitutive modeling and experiments.

This strain recovery is now commonly termed "shape-memory" phenomenon and was firstly introduced in the mid of the last century. It is only from the past twenty years that the research on shape-memory polymers has seen an explosive growth in both academics and industrial fields (Lendlein and Kelch, 2002; Hu et al., 2012; Zhao et al., 2015). They are merged as a new class of self-repairing and intelligent materials with a very wide range of potential application areas from biomedical engineering for minimal invasive surgery to aerospace industry. Nonetheless, all polymers have a thermally-induced shape-memory capacity even under large-strains. The shape-memory behavior of a polymer is due to the flexibility of the polymer chains and their capacity to store and release mechanisms through treatments around a defined transition temperature. For amorphous networks, the transition temperature is the glass transition temperature T_g. The thermally-activated shape-memory effect may be evidenced using conventional techniques as visualized in Figure 1 when the polymer specimen passes through four steps to form a cycle with different temporary states from the initial state I to the recovered state V[1]. The compression is chosen because of the homogeneous nature of this deformation mode within large deformation behavior. Below T_g, the glassy specimen is compressed at a given strain-rate $\dot{\varepsilon}$ to the desired strain (state II) in which the post-yield response is strongly nonlinear and generally governed by two features: a strain-softening immediately after yield-peak followed by a strain-hardening at large-strains. The specimen is then unloaded down to zero-stress $\sigma = 0$ at the same absolute strain-rate $\dot{\varepsilon}$ (state III). Upon unloading, a part of the stored energy is released. The nonlinearity in unloading is indicative of the instantaneous recovery of an amount of the inelastic strain beyond that associated with the linear elasticity. At the end of the unloading process, a substantial remanent strain is retained which necessitates a very long recovery time as long as the temperature is held constant. To activate the recovery process, the deformed specimen is firstly cooled down to room temperature T_0 (state IV) in a mechanical loading free condition and then reheated above T_g under zero-stress (state V). The recovery process is strongly dependent on the previous thermo-mechanical history (temperature, strain-level and strain-rate) and the heating conditions in terms of recovery temperature and heating rate.

The constitutive model of Haward and Thackray (1968), extended later by Boyce et al. (1988) into a 3-D finite strain formulation, appears to be the first effort to formulate a constitutive theory for amorphous thermoplastics below their glass transition temperature and has been early developed based on the observation of the recovery. It has been the inspiration of a multitude of constitutive models for the time-temperature dependence of the yielding behavior in continuum terms invoking mechanical analogs by using combinations of elements, usually linear elastic springs, viscoplastic dashpots and nonlinear elastic springs (Arruda et al., 1995; Buckley and Jones, 1995; Tervoort et al., 1997; Boyce et al., 2000; Lion, 2000; Richeton et al., 2007; Ames et al., 2009; Anand et al., 2009; Belbachir et al., 2010; Srivastava et al., 2010a; Zaïri et al., 2010, 2011; Bouvard et al., 2013; Bouaksa et al., 2014; Nguyen et al., 2016; Gudimetla and Doghri, 2017; Mahjoubi et al., 2019, 2020). As a common point, a hyperelastic strain-hardening resistance is associated to an elastoviscoplastic formulation to account for the intermolecular resistance. Mathematically, the connection between both resistances vary from a model to another and is realized either by considering the orientation

[1] The shape-memory behavior is widely studied by a sequence of heating, deformation (in the rubbery state), cooling (with the deformation maintained) and unloading (in the glassy state); the heating closes the shape-memory loop. The latter shape-memory cycle procedure is called hot programming within the shape-memory community (Dai et al., 2020). By contrast, a cold programming (Dai et al., 2020) is preferred here. It consists to a sequence of deformation, unloading (in the glassy state), cooling and heating (in the rubbery state under zero-stress creep) in order to highlight the importance of the elastoviscoplastic behavior in the glassy state.

hardening as a kinematic back-stress or as an additive stress. Physically, the models consider generally that the orientation hardening originates from the rubber-elastic response of the macromolecular chains between junctions in the macromolecular network that persist through a temperature range, called physical entanglements in the case of an amorphous thermoplastic and frozen in when it is cooled from the melt state. The concept of physical entanglements and rubber-elastic analogy in glassy polymers is now commonly accepted to explain the strain-hardening at large-strains. The strongest argument is the increase of the strain-hardening with the entangled polymer network density due to enhanced straightening out of chains between entanglements and associated orientation of the macromolecular network. The stress contribution of the orientation hardening is generally constitutively described using the rubber-elastic network theories where the cross-links play the role of junctions in the macromolecular network. The effort of modeling for amorphous thermoplastics continues to date, but it is generally focused on the reproduction of the stress-strain behavior, sometimes spanning the glass transition temperature, but generally without being interested in the thermally-induced shape-memory capacity.

The earlier modeling attempts to describe the thermally-activated recovery effects are due to Tobushi et al. (1997, 2001) and Lin and Chen (1999) studying shape-memory polyurethane based-polymers in the framework of thermo-viscoelasticity combined with a frictional element. Later, two main classes of models have been proposed to capture the thermally-induced shape-memory behavior of amorphous polymers considering either the viscosity temperature-change approach (Diani et al., 2006; Nguyen et al., 2008; Castro et al., 2010; Srivastava et al., 2010b; Chen and Nguyen, 2011; Su and Peng, 2018; Mao et al., 2019) or the rubbery-glassy phase-transition approach (Liu et al., 2006; Chen and Lagoudas, 2008a, 2008b; Qi et al., 2008; Ghosh and Srinivasa, 2013, 2014; Boatti et al., 2016; Park et al., 2016; Yang and Li, 2016; Li et al., 2017). The first class of models introduces the temperature-dependence of the molecular mobility and the relaxation time. The second class of models is the widely used approach due to its simplicity. It introduces a phase-transition hypothesis considering the amorphous network as a continuum mixture of a glassy phase and a rubbery phase using the concept of phase volume fraction to describe the evolution of the microstructure. The glassy and rubbery phases are stable below and above the transition temperature, respectively, and the transitions between the two superimposed phases with a temperature change provide a description of the strain storage and recovery during a shape-memory cycle. The phase-transition approach, originally developed for shape memory alloys, finds a strong physical meaning when the shape-memory behavior concerns polymer medium with a phase transformation, i.e. crystallizable polymers (Guo et al., 2018a; Moon et al., 2019). In an original amorphous medium that remains amorphous, the phase-transition approach remains conceptual and the lack of physical meaning constitutes the main limitation. Most of models deal with the thermally-induced shape-memory of thermoplastic elastomers or thermoset polymers and are limited to certain classes of constitutive responses.

Our approach differs from the above models. With the aim of developing an approach that is as general as possible and physically-based, the presented elastoviscoplastic-viscohyperelastic model includes the variation of the intermolecular and network properties with temperature and their abrupt change when the temperature traverses the glass transition temperature. The constitutive equations combine existing elements from several theories (elasticity, viscoplasticity and viscohyperelasticity) that are presented in a unifying manner and in a new way according to the model structure in order to facilitate finding the key to the thermally-activated strain recovery in connection with the microstructure and to give a clearer definition of the "plasticity" in amorphous polymer systems. Our approach is simplest than previous models and does not need to consider sub-networks and the introduction of an additional mathematical formulation for strain recovery during heating. While our approach remains

enough simple, it is based upon a physical understanding of the material behavior by considering the underlying thermo-mechanical mechanisms and their abrupt change in the temperature dependence when the material changes from the glassy state to the rubbery state. For the development of the thermo-mechanical model, compression experiments on a polycarbonate were conducted over a wide range of temperatures across the transition temperature. The model prediction is studied for zero-stress creep recovery.
The present paper is organized as follows. In Section 2, the finite strain constitutive theory is presented in the nonlinear continuum thermo-mechanical framework[2]. In Section 3, the attention is devoted to the quality of the model fit to the experimental stress-strain curves and to the predictive model capability for recovery response. We close in Section 4 with final remarks.

2. Theory

The apparent plasticity is regarded as a thermally-activated process determined by elementary molecular events related to intermolecular and intramolecular motions, the thermally-activated recovery being made possible by the introduction of their variation with temperature. Figure 2 provides a schematic view of an amorphous network along with the elementary molecular events occurring inside. The restriction imposed on molecular chain motion due to neighboring chains leads to intermolecular interactions resulting in a first resistance to small-moderate deformations. The latter resistance (intermolecular resistance *I*) is responsible for the initial stiffness and the yield events. At larger deformations, the orientation and relaxation processes of the macromolecular network lead to a second resistance (molecular network resistance *N*) responsible for the remarkable strain-hardening response.

2.1. Molecular events and properties

It is now well agreed that the glass transition is the key physical feature for the shape-memory effects of amorphous networks. Nonetheless, this subsection introduces fundamental relations between all elementary molecular events and properties for the sake of completeness in the description of polymer deformation. The nature of the molecular mobility in amorphous thermoplastics results from intermolecular barriers to chain-segment rotation of two distinct molecular sub-segments related to thermally-activated α and β processes acting at two different levels[3]. The activation energy required for the very local movement of the β process is low, and its relaxation is activated before the α process. The two relaxations are key features for the polymer deformation and a physically consistent description is needed. An Arrhenius-type expression describes the strain-rate dependence of the β transition temperature (Richeton et al., 2005b):

$$\frac{1}{T_\beta\left(\dot{\varepsilon}\right)}=\frac{1}{T_{\beta ref}}+\frac{k}{\Delta H_\beta}\ln\left(\frac{\dot{\varepsilon}_{ref}}{\dot{\varepsilon}}\right) \tag{1}$$

in which $T_{\beta ref}$ is the β transition temperature at the chosen reference strain-rate $\dot{\varepsilon}_{ref}$, ΔH_β is the activation energy required for the local movement of the β process and k is the Boltzmann's constant.

---

[2] The following notation is used throughout the text. Tensors and vectors are denoted by normal boldfaced letters and italicized boldfaced letters, respectively, while scalars and individual components of vectors and tensors are denoted by normal italicized letters. The superposed dot expresses the time derivative. The term *tr* denotes trace. The superscript *T* denotes the transpose.

[3] In the specific case of polycarbonate, the α and β processes are associated to the rotation of the polymer main chain and the phenyl group, respectively.

The α transition is also referred to as the glass transition which follows the Williams-Landel-Ferry (WLF) free-volume theory (Richeton et al., 2005b):

$$T_g\left(\dot{\varepsilon}\right) = T_{gref} - c_{2g}\log\left(\frac{\dot{\varepsilon}_{ref}}{\dot{\varepsilon}}\right)\left(c_{1g} + \log\left(\frac{\dot{\varepsilon}_{ref}}{\dot{\varepsilon}}\right)\right)^{-1} \tag{2}$$

in which T_{gref} is the α transition temperature at $\dot{\varepsilon}_{ref}$ and, c_{1g} and c_{2g} are the WLF coefficients.

To complete the description of the temperature variation, the melting temperature T_m is described by a phenomenological formula (Richeton et al., 2005b):

$$T_m\left(\dot{\varepsilon}\right) = T_{mref}\left(1 + 10^{-2}\log\left(\frac{\dot{\varepsilon}}{\dot{\varepsilon}_{ref}}\right)\right) \tag{3}$$

in which T_{mref} is the melting transition temperature at $\dot{\varepsilon}_{ref}$.

The elasticity and the plastic yielding of amorphous thermoplastics are strongly affected by strain-rate and temperature, with a similar dependency. As shown in Figures 3a and 3b, these two quantities decrease with temperature and increase with strain-rate. The latter effects must be correlated to the transition temperatures. The variation of the Young's modulus E with temperature θ and strain-rate $\dot{\varepsilon}$ is given by the following expression, valid from fully glassy state to fully rubbery state (Richeton et al., 2005b):

$$E\left(\theta,\dot{\varepsilon}\right) = E_{T_\beta}\left(\theta,\dot{\varepsilon}\right) + E_{T_g}\left(\theta,\dot{\varepsilon}\right) + E_{T_m}\left(\theta,\dot{\varepsilon}\right) \tag{4}$$

in which the terms $E_{T_\beta}\left(\theta,\dot{\varepsilon}\right)$, $E_{T_g}\left(\theta,\dot{\varepsilon}\right)$ and $E_{T_m}\left(\theta,\dot{\varepsilon}\right)$ correspond to three parts around the main transitions: β relaxation, α relaxation (glass transition) and melting which are characterized by their transition temperatures, T_β, T_g and T_m. The three parts are described by the following formulae using Weibull statistics (Richeton et al., 2005b):

$$E_{T_\beta}\left(\theta,\dot{\varepsilon}\right) = \left(E_1\left(\dot{\varepsilon}\right) - E_2\left(\dot{\varepsilon}\right)\right)\exp\left(-\left(\frac{\theta}{T_\beta\left(\dot{\varepsilon}\right)}\right)^{m_1}\right) \tag{5}$$

$$E_{T_g}\left(\theta,\dot{\varepsilon}\right) = \left(E_2\left(\dot{\varepsilon}\right) - E_3\left(\dot{\varepsilon}\right)\right)\exp\left(-\left(\frac{\theta}{T_g\left(\dot{\varepsilon}\right)}\right)^{m_2}\right) \tag{6}$$

$$E_{T_m}\left(\theta,\dot{\varepsilon}\right) = E_3\left(\dot{\varepsilon}\right)\exp\left(-\left(\frac{\theta}{T_m\left(\dot{\varepsilon}\right)}\right)^{m_3}\right) \tag{7}$$

where m_1, m_2 and m_3 are the Weibull shape parameters of each transition region and, $E_1\left(\dot{\varepsilon}\right)$, $E_2\left(\dot{\varepsilon}\right)$ and $E_3\left(\dot{\varepsilon}\right)$ are the instantaneous moduli at the beginning of each transition region (Richeton et al., 2005b):

$$E_1\left(\dot{\varepsilon}\right) = E_{1ref}\left(1 + s\log\left(\frac{\dot{\varepsilon}}{\dot{\varepsilon}_{ref}}\right)\right) \tag{8}$$

$$E_2\left(\dot{\varepsilon}\right) = E_{2ref}\left(1 + s\log\left(\frac{\dot{\varepsilon}}{\dot{\varepsilon}_{ref}}\right)\right) \tag{9}$$

$$E_3\left(\dot{\varepsilon}\right) = E_{3ref}\left(1 + s\log\left(\frac{\dot{\varepsilon}}{\dot{\varepsilon}_{ref}}\right)\right) \tag{10}$$

where E_{1ref}, E_{2ref} and E_{3ref} are the instantaneous moduli at a chosen reference strain-rate $\dot{\varepsilon}_{ref}$ and, s is a parameter characterizing the strain-rate sensitivity of the stiffness modulus assumed to be the same for the three transition regions.

Figure 3a presents the Young's modulus variation with temperature of polycarbonate, using the above equations, from fully glassy state to fully rubbery state. In the isotropic case, the elasticity may be completely defined by the Young's modulus E and the Poisson's ratio ν. The latter material property was assumed to be strain-rate independent but temperature dependent[4]:

$$\nu\left(\theta\right) = 0.36 + 0.139\exp\left(\frac{\theta - \left(2\left(T_{gref} + 10.3 - \theta\right)\right)^2}{T_{gref} + 10.3}\right) \text{ for } \theta < T_g \tag{11}$$

below T_g, and

$$\nu\left(\theta\right) = 0.499 \text{ for } \theta \geq T_g \tag{12}$$

above T_g.

Once the energy barrier to molecular mobility is overcome the elastic behavior gives way to the plastic yielding through the thermally-activated local rotation of molecular segments. Figure 3b presents the yield stress variation with temperature of polycarbonate from fully glassy state to fully rubbery state. At low temperatures, the increase of the yield strength with strain-rate is correlated to the decrease of the molecular mobility leading to the stiffening of the chains. This increase of the yield strength is associated to the activation of both α and β processes. However, at high temperatures and low strain-rates, the intermolecular resistance is mainly due to the α process while the β process is hind. The physics of plastic yielding is described by the accumulated viscoplastic strain rate $\dot{\gamma}_I^{\text{vp}}$ that differs on both sides of T_g:

$$\dot{\gamma}_I^{\text{vp}} = \hat{\dot{\gamma}}_I^{\text{vp}}\left(\Delta H_\beta, V, \sigma_{\text{int}}\right) \text{ for } \theta < T_g \tag{13}$$

below T_g, and

$$\dot{\gamma}_I^{\text{vp}} = \hat{\dot{\gamma}}_I^{\text{vp}}\left(\Delta H_\beta, V\right) \text{ for } \theta \geq T_g \tag{14}$$

above T_g.

The term ΔH_β is again the β activation energy, V is an activation volume and σ_{int} is the internal intermolecular stress frozen in the deformed network in the glassy state (see Figure 2). The internal stress evolves from its initial value $\sigma_{\text{int}(t=0)}$ to the value σ_{ps} referring to the preferred structural state of the polymer chains according to the following evolution law:

$$\dot{\sigma}_{\text{int}} = h\left(1 - \frac{\sigma_{\text{int}}}{\sigma_{ps}}\right)\dot{\gamma}_I^{\text{vp}} \tag{15}$$

The evolution (15) is introduced to account for the strain-softening response in the glassy state manifested by a drop in stress with strain upon initiation of the plastic flow. The term h

[4] Typical values of polycarbonate are used.

is the strain-softening slope. The ratio $\sigma_{\text{int}(t=0)}/\sigma_{ps}$ is assumed constant and the temperature dependence of $\sigma_{\text{int}(t=0)}$ is given by a linear law (Richeton et al., 2006):

$$\sigma_{\text{int}(t=0)} = \sigma_{\text{int}(\theta=0)} - m\theta + \alpha\sigma_{Im} \tag{16}$$

where $\sigma_{\text{int}(\theta=0)}$ is the internal intermolecular stress at the temperature θ = 0 K, m is the sensitivity parameter vis-à-vis the temperature and α is the sensitivity parameter vis-à-vis the intermolecular mean stress σ_{Im}.

At larger deformations, the molecular network experiences an orientation process leading to the rapid stress increase at the macroscopic scale. The latter material feature is directly related to the limiting extensibility of the molecular network and can be identified by two physical ingredients: the initial hardening modulus $C_r = n_c k\theta$ (n_c is the average number of chains per unit volume) and the average number of rigid links N_{rl} between physical molecular chain entanglements. As shown in Figure 3c, the variation with temperature of the two parameters differs on both sides of T_g. According to experimental observations of G'sell and Souami (1997) on the hardening modulus variation with temperature of amorphous networks, the parameter C_r decreases below T_g and increases above T_g, whereas the parameter N_{rl} increases below T_g and is constant above T_g. The following kinetics is then retained (Richeton et al., 2007):

$$\begin{aligned} C_r &= C_{r0} - a\theta \\ N_{rl} &= N_{rl0} + b\theta \end{aligned} \quad \text{for } \theta \le T_g \tag{17}$$

below T_g, and

$$\begin{aligned} C_r &= \left(C_{r0} - aT_g\right)\frac{\theta}{T_g} \\ N_{rl} &= N_{rl0} + bT_g \end{aligned} \quad \text{for } \theta \ge T_g \tag{18}$$

above T_g.

The terms C_{r0}, N_{rl0}, a and b are constants in the kinetics (17) and (18). The different behavior of C_r and N_{rl} on both sides of the glass transition is due to relative importance of internal energy and entropic effect in the glassy state and in the rubbery state. Richeton et al. (2007) used the same kinetics (17) and (18) for the orientation hardening but by introducing them in a kinematic back-stress. In addition, the entangled molecular network orientation process translated by the kinetics (17) and (18) enters in competition with the molecular network relaxation process due to chain reptation allowing decreasing the stress[5]. The physics of molecular network relaxation is described by the accumulated viscous strain rate $\dot{\gamma}_N^v$:

$$\dot{\gamma}_N^v = \hat{\dot{\gamma}}_N^v\left(C\right) \tag{19}$$

As presented in Figure 3c, the term C is a viscosity parameter that linearly increases with temperature with the same slope on both sides of the glass transition (Zaïri et al., 2010):

$$C = C_0 + c\theta \tag{20}$$

where C_0 and c are constants.

[5] As one of the most successful theory in polymer physics, Doi and Edwards (1986) introduced the concept of the reptational Brownian motion: A macromolecule can be thought as trapped in a tube-like region where it can move in a snake-like fashion while having its lateral movements restricted. In an amorphous thermoplastic, the latter is due to the presence of neighboring chains and physical entanglements in the macromolecular network.

2.2. Constitutive equations

This subsection presents constitutive relationships between the macro-stress response and the set of physically-interpretable material parameters introduced above along with their remarkable change when the temperature traverses the glass transition. The model is developed from the concept that the intermolecular resistance *I* and the molecular network resistance *N* participate to the total resistance to deformation in polymers by acting in parallel. The total Cauchy stress $\boldsymbol{\sigma}$ is thus the sum of both contributions:

$$\boldsymbol{\sigma} = \boldsymbol{\sigma}_I + \boldsymbol{\sigma}_N \tag{21}$$

The two basic physical mechanisms are, respectively, formulated using the elastoviscoplastic theory, to reproduce the initial stiffness and the yield events, and the viscohyperelastic theory, to reproduce the remarkable strain-hardening at large-strains[6]. The general form of the model is illustrated schematically in Figure 2 for a one-dimensional visualization analog of the polymer deformation model: the resistance *I* is constituted by a linear spring in series with a viscoplastic damper and, the resistance *N* is constituted by a hyperelastic spring in series with a viscous damper. The two resistances, acting in parallel, are joined in series to a thermal branch responsible for the stress-free thermal expansion. The corresponding kinematics of large-strain thermo-mechanics is recalled in Appendix A.

The intermolecular Cauchy stress $\boldsymbol{\sigma}_I$ is expressed as a function of the corresponding strain by the following constitutive relationship with linear spring analog:

$$\boldsymbol{\sigma}_I = \frac{\mathbf{C}_I^{\mathrm{e}}}{J_I} \ln\left(\mathbf{V}_I^{\mathrm{e}}\right) \tag{22}$$

where $J_I = \det\left(\mathbf{F}_I^e\right)$ represents the elastic volume change and $\ln\left(\mathbf{V}_I^{\mathrm{e}}\right)$ is the Hencky elastic strain (see Appendix A). The elastic stiffness tensor $\mathbf{C}_I^{\mathrm{e}}$ is expressed in terms of the Young's modulus E and the Poisson's ratio ν as follows:

$$\left(\mathbf{C}_I^e\right)_{ijkl} = \frac{E\left(\theta,\dot{\varepsilon}\right)}{2\left(1+\nu\left(\theta\right)\right)}\left[\left(\delta_{ik}\delta_{jl}+\delta_{il}\delta_{jk}\right)+\frac{2\nu\left(\theta\right)}{1-2\nu\left(\theta\right)}\delta_{ij}\delta_{kl}\right] \tag{23}$$

in which the term δ denotes the Kronecker-delta symbol.

The network Cauchy stress $\boldsymbol{\sigma}_N$ is expressed as a function of the corresponding strain with hyperelastic spring analog. It is constitutively expressed using a rubber-elastic network formulation introducing the initial hardening modulus C_r and the average number of rigid links N_{rl}. The Arruda-Boyce 8-chain model is used (Arruda and Boyce, 1993):

$$\boldsymbol{\sigma}_N = \frac{1}{J_N}\frac{C_r\left(\theta\right)}{3}\frac{\sqrt{N_{rl}\left(\theta\right)}}{\bar{\lambda}_N^{\mathrm{h}}} L^{-1}\left(\frac{\bar{\lambda}_N^{\mathrm{h}}}{\sqrt{N_{rl}\left(\theta\right)}}\right)\left[\bar{\mathbf{F}}_N^{\mathrm{h}}\left(\bar{\mathbf{F}}_N^{\mathrm{h}}\right)^T-\left(\bar{\lambda}_N^{\mathrm{h}}\right)^2\mathbf{I}\right] \tag{24}$$

in which $J_N = \det\left(\mathbf{F}_N^{\mathrm{h}}\right)$ represents the network volume change, $\bar{\lambda}_N^{\mathrm{h}} = \sqrt{\mathrm{tr}\left(\bar{\mathbf{F}}_N^{\mathrm{h}}\left(\bar{\mathbf{F}}_N^{\mathrm{h}}\right)^T\right)/3}$ is the average hyperelastic network stretch on a chain where $\bar{\mathbf{F}}_N^{\mathrm{h}} = \left(J_N\right)^{-1/3}\mathbf{F}_N^{\mathrm{h}}$ and $\mathbf{I}$ is the identity tensor. The inverse Langevin function is given by a Padé approximation: $\mathrm{L}^{-1}\left(x\right) \approx x\left(3-x^2\right)/\left(1-x^2\right)$. The deformation $\mathbf{F}_N^{\mathrm{h}}$ in the hyperelastic spring drives Eq. (24) via the interaction with the deformation $\mathbf{F}_N^{\mathrm{v}}$ in the viscous damper (see Appendix A).

---

[6] The superscripts e, vp, h and v denote the elastic, viscoplastic, hyperelastic and viscous contributions, respectively.

The viscoplastic stretching rate tensor $\mathbf{D}_I^{\mathrm{vp}}$, and its alter ego, the viscous stretching rate tensor $\mathbf{D}_N^{\mathrm{v}}$, are given by the following flow rules:

$$\mathbf{D}_I^{\mathrm{vp}} = \dot{\gamma}_I^{\mathrm{vp}} \frac{\boldsymbol{\sigma}'_I}{\sqrt{2}\left\|\boldsymbol{\sigma}_I\right\|},\ \left\|\boldsymbol{\sigma}_I\right\| = \sqrt{\frac{\mathrm{tr}\left(\boldsymbol{\sigma}'_I \boldsymbol{\sigma}'^T_I\right)}{2}} \tag{25}$$

$$\mathbf{D}_N^{\mathrm{v}} = \dot{\gamma}_N^{\mathrm{v}} \frac{\boldsymbol{\sigma}'_N}{\sqrt{2}\left\|\boldsymbol{\sigma}_N\right\|},\ \left\|\boldsymbol{\sigma}_N\right\| = \sqrt{\frac{\mathrm{tr}\left(\boldsymbol{\sigma}'_N \boldsymbol{\sigma}'^T_N\right)}{2}} \tag{26}$$

in which $\dot{\gamma}_I^{\mathrm{vp}}$ and $\dot{\gamma}_N^{\mathrm{v}}$ are the accumulated viscoplastic and viscous strain rates, $\left\|\boldsymbol{\sigma}_I\right\|$ and $\left\|\boldsymbol{\sigma}_N\right\|$ are the effective shear stresses related to the deviatoric part of the intermolecular Cauchy stress and of the network Cauchy stress, respectively: $\boldsymbol{\sigma}'_I = \boldsymbol{\sigma}_I - \sigma_{Im}\mathbf{I}$ with $\sigma_{Im} = \mathrm{tr}\left(\boldsymbol{\sigma}_I\right)/3$ the intermolecular mean stress and $\boldsymbol{\sigma}'_N = \boldsymbol{\sigma}_N - \sigma_{Nm}\mathbf{I}$ with $\sigma_{Nm} = \mathrm{tr}\left(\boldsymbol{\sigma}_N\right)/3$ the network mean stress.

For the accumulated viscoplastic strain rate $\dot{\gamma}_I^{\mathrm{vp}}$, the mathematical formulation of Richeton et al. (2006, 2005a) is retained:

$$\dot{\gamma}_I^{\mathrm{vp}} = \dot{\gamma}_0 \exp\left(-\frac{\Delta H_\beta}{R\theta}\right)\sinh^n\left(\frac{\left(\left\|\boldsymbol{\sigma}_I\right\| - \sigma_{\mathrm{int}}\right)V}{2k\theta}\right) \quad \text{for } \theta < T_g \tag{27}$$

below T_g, and

$$\dot{\gamma}_I^{\mathrm{vp}} = \dot{\gamma}_0 \exp\left(-\frac{\Delta H_\beta}{RT_g}\right)\exp\left(\frac{\ln 10 \times c_{1g}\left(\theta - T_g\right)}{c_{2g} + \theta - T_g}\right)\sinh^n\left(\frac{\left\|\boldsymbol{\sigma}_I\right\| V}{2k\theta}\right) \quad \text{for } \theta \geq T_g \tag{28}$$

above T_g.

The term $\dot{\gamma}_0$ is the pre-exponential factor, R is the perfect gas constant and n is a parameter characterizing the cooperative movement of the chain segments. The time-temperature dependence of the orientation hardening at large-strains is constitutively described using the expression (24) for the entangled polymer network orientation process combined with a viscous formulation for the relaxation process. The accumulated viscous strain rate $\dot{\gamma}_N^{\mathrm{v}}$ is formulated within a viscoplastic theory with no yield surface (Pyrz and Zaïri, 2007), the viscous deformation being non-zero from the beginning of the mechanical loading. Motivated by the concept of the reptational Brownian motion, the Bergstrom-Boyce power law expression for stress/strain-assisted molecular network relaxation rate is retained (Bergstrom and Boyce, 1998):

$$\dot{\gamma}_N^{\mathrm{v}} = C\left(\theta\right)\left|\lambda_N^{\mathrm{v}} - 1\right|^{-1}\left\|\boldsymbol{\sigma}_N\right\| \tag{29}$$

where $\lambda_N^{\mathrm{v}} = \sqrt{\mathrm{tr}\left(\mathbf{F}_N^{\mathrm{v}}\left(\mathbf{F}_N^{\mathrm{v}}\right)^T\right)/3}$ is the viscous network stretch with an initial value that deviates slightly from 1.0 in the computations to avoid singularity.

2.3. Thermally-activated strain recovery

Figure 4 presents the loading-unloading-recovery process applied to the specimen. At the glassy state ($\theta < T_g$), the macromolecular chains have low mobility, so that the intermolecular resistance I is enhanced and the material stores a substantial remanent strain when the mechanical loading is removed as illustrated in Figure 1. The amount of this apparent plastic deformation depends on the temperature and the strain-rate. In this unloaded state, the elastic

intermolecular deformation is totally recovered, i.e. $\mathbf{F}_I^{\mathrm{e}} = \mathbf{I}$, and the internal intermolecular stress σ_{int} is frozen in the material. An amount of the network deformation $\mathbf{F}_N$ is also recovered (due to the parallelism of intermolecular and network resistances) which leads to the stress nonlinearity upon unloading, the remaining network deformation contributing to the remanent strain. When the polymer is cooled down to room temperature ($\theta = T_0$), it becomes in complete frozen state and the total stress $\boldsymbol{\sigma}$ becomes null. Then, Eq. (21) writes:

$$\boldsymbol{\sigma}_I + \boldsymbol{\sigma}_N = \mathbf{0} \text{ at } \theta = T_0 \tag{30}$$

with $\mathbf{F}_I^{\mathrm{vp}} \neq \mathbf{I}$ and $\mathbf{F}_N \neq \mathbf{I}$. By considering volume preserving and irrotationality of the inelastic flow (see Appendix A), the intermolecular stress $\boldsymbol{\sigma}_I$ may be obtained by combining Eqs. (25) and (27):

$$\boldsymbol{\sigma}_I = \frac{\sqrt{2}}{\dot{\gamma}_I^{\mathrm{vp}}}\left(\frac{2k\theta}{V}\operatorname{arsinh}\left(\frac{\dot{\gamma}_I^{\mathrm{vp}}}{\dot{\gamma}_0}\exp\left(\frac{\Delta H_\beta}{R\theta}\right)\right)^{1/n} + \sigma_{\mathrm{int}}\right)\dot{\mathbf{F}}_I^{\mathrm{vp}}\mathbf{F}_I^{\mathrm{vp}^{-1}} \tag{31}$$

in which $\mathbf{D}_I^{\mathrm{vp}} = \dot{\mathbf{F}}_I^{\mathrm{vp}}\mathbf{F}_I^{\mathrm{vp}^{-1}}$ and $\mathbf{F}_I^{\mathrm{e}} = \mathbf{I}$.

In Eq. (30), the network stress $\boldsymbol{\sigma}_N$ is given by Eq. (24). Inherent to its formulation, the model considers that the two resistances act in parallel and without interaction. Nonetheless, a correlation exists between intermolecular and network properties. Indeed, as shown in Figures 3a, 3b and 3c, the kinetics with temperature increase is due to increase in molecular mobility, chain orientation and relaxation process. At the rubbery state ($\theta > T_g$), the macromolecular chains can undergo large random conformational motions which increase their mobility, such that the intermolecular resistance *I* becomes negligible. More precisely, the response is governed by the orientation/relaxation network resistance *N*. In this region, the macromolecular chains are dominated by entropy as indicated by the increase of C_r in the right side of the glass transition. Also, the chain viscosity translated by C is important: in this region, the macromolecular chains slide more easily against each other and take the capability to significantly change conformation by Brownian motion in a combination of reptation motion, as considered in the Doi-Edwards concept and constitutively represented by Eq. (29). The shape-memory behavior is therefore a consequence of a remarkable change in thermo-mechanical properties at the chain-scale in response to a temperature change. In particular, during the heating process from glassy state up to rubbery state, the inelastic features change quickly in response to a temperature variation.

As the true stress-strain curves, the recovery response may be considered as an intrinsic feature obtained by the following zero-stress creep condition above glass transition:

$$\boldsymbol{\sigma}_I + \boldsymbol{\sigma}_N = \mathbf{0} \text{ and } \theta > T_g \tag{32}$$

where the intermolecular stress $\boldsymbol{\sigma}_I$ is again expressed by Eq. (31) and the network stress $\boldsymbol{\sigma}_N$ by Eq. (24). The accumulated viscoplastic strain rate $\dot{\gamma}_I^{\mathrm{vp}}$ in Eq. (31) is governed by Eq. (28) in which $\boldsymbol{\sigma}_I$ is replaced by $-\boldsymbol{\sigma}_N$ according to the condition (32). Note that $\|\boldsymbol{\sigma}_I\| = \|\boldsymbol{\sigma}_N\|$. Via the material kinetics of Section 2.1 introduced in Eq. (32), the model makes possible to consider that the deformed macromolecular structure keeps "memory" of its original position during heating above glass transition, the network resistance being used as the driving stress that continuously activates the recovery process during zero-stress creep above glass transition. By this way, the polymer regains the entropy that was lost during the chain orientation and relaxes to an equilibrium configuration in which it recovers in a great extent the initial conformation by "memory" effect. To further illustrate our approach, the viscoplastic intermolecular stretch is plotted as a function of the viscous network stretch in

Figure 4. The increase in plastic strain during isothermal mechanical loading ($\mathrm{I} \rightarrow \mathrm{II}$) is followed by a frozen process during unloading ($\mathrm{II} \rightarrow \mathrm{III}$). The heating above glass transition combined with zero-stress creep ($\mathrm{IV} \rightarrow \mathrm{V}$) metamorphoses the apparent plasticity into a recoverable process while the viscous network stretch exhibits continuous creep behavior as a manifestation of the reptational Brownian motion.

3. Application to polycarbonate

3.1. Experiments

A series of experimental tests have been performed on polycarbonate cylinders to get the stress-strain and recovery response assessing the thermally-induced shape-memory cycle as already illustrated in Figure 1. The experiments were carried out on an electromechanical model-5567 Instron universal testing machine equipped with an oven. Cylindrical specimens of 8.00 mm length and 6.3 mm diameter were machined from polycarbonate cylinders purchased from Goodfellow[7]. The length to-diameter ratio of the specimens allows getting the stress-strain response at large-strains by avoiding both buckling and non-homogeneous deformation. Lubricant was used between the compression platens and the specimen surfaces (smooth and parallel) to avoid both barreling and shearing phenomena during the compression. Three kinds of tests were performed:

- Loading-unloading tests at different strain-rates and temperatures: The specimens were uniaxially loaded at a constant strain-rate until a prescribed strain and then unloaded at the same absolute strain-rate until zero-stress. The tests were conducted at three strain-rates $\dot{\varepsilon}$ (0.01 s^{-1}, 0.001 s^{-1} and 0.0001 s^{-1}) over a wide range of compression temperatures θ: 298 K, 333 K, 363 K, 393 K and 433 K. This experiment reproduces the behavior of the states I, II and III in Figure 1.
- Zero-stress creep recovery above glass transition: The specimens, previously compressed below T_g, were cooled down to room temperature by natural cooling and then submitted to creep experiments at zero-stress for two heating temperatures: 433 K (T_g + 10 K) and 473 K (T_g + 50 K). This experiment reproduces the behavior of the states IV and V in Figure 1. The recovery R will be defined as:

$$R = \left(1 - \frac{\varepsilon}{\varepsilon_{\max}}\right) \times 100 \tag{33}$$

  where ε and $\varepsilon_{\max}$ are, respectively, the remanent strain stored in the material and its maximum value.
- Successive constant-temperature loading-unloading tests below glass transition: The specimens were successively compressed until a prescribed strain at four temperatures: 298 K, 333 K, 363 K and 393 K. Between each loading-unloading test, the compressed specimen was cooled down to room temperature by natural cooling. The strain was small enough (10%) to avoid orientation hardening and the strain-rate was fixed to 0.001 s^{-1}. Two cases were considered: increasing compression temperatures from 298 K to 393 K and decreasing compression temperatures from 393 K to 298 K.

In what follows, the temperature and strain-rate dependent loading-unloading results are used to obtain the kinetics of the model constants while the successive constant-temperature loading-unloading results and the thermally-activated recovery results serve to verify the model predictive capabilities.

[7] The reference glass transition is 423 K and the reference melting temperature is 493 K. These are typical values for polycarbonate (Neki and Geil, 1973).

3.2. Model fit

Figure 5 presents the deformation behavior of polycarbonate for different temperatures and strain-rates, up to a true strain-level of 70%. The polymer exhibits the expected dependencies on temperature with two distinct responses below and above the glass transition. A zoom is provided in Figure 5d for the highest compression temperature. Below the glass transition, the material exhibits the stress-strain behavior characteristics of a typical amorphous thermoplastic in the glassy state from small to large-strains. The strain-rate affects the plastic flow stress (yield-peak and strain-softening) but both stiffness modulus and hardening modulus present a relatively weak dependence on strain-rate. The plastic flow stress drops significantly upon a temperature increase. The remanent strain, for which stress is zero at unloading, is slightly affected by the temperature. When the temperature increases further and exceeds the glass transition, the polymer exhibits a very low yield strength and responds as a hysteretic-rubber-like material for which the material viscosity is still significant as evidenced by the strain-rate dependency. The remanent strain is significantly different as the strain-rate changes. Furthermore, it can be noticed that the remanent strain seems higher than that generally observed for cross-linked network systems such as rubbers (e.g. Guo et al., 2018d).

The intermolecular and network constants are identified separately thanks to the model structure. The intermolecular properties are mainly defined by the stiffness modulus and the yield strength. They are plotted in Figures 3a and 3b as a function of temperature in the form of symbols. The first quantity is deduced from the initial slope of the stress-strain curve. The second quantity is deduced from the zero slope of yield-peak below the glass transition and the linear deviation above the glass transition. The stiffness modulus remains almost constant in the glassy region whereas the yield stress decreases monotonically with temperature. Both quantities change abruptly when the temperature traverses the glass transition. Table 1 provides the values of the model constants. The glassy-rubbery stiffness variation with temperature allowed identifying the model constants in Eqs. (1)-(10). A reference strain-rate $\dot{\varepsilon}_{ref}$ of 1 s^{-1} was used. The model constants in Eqs. (16), (27) and (28) were extracted by means of a least-square adjustment of the yield stress as a function of temperature and over a range of strain-rates. The model constants in Eq. (15) were determined by fitting the model to the strain-softening region of the stress-strain data in the glassy state. Although, they were assumed constant vis-à-vis temperature, the model accounts for the temperature dependence of the strain-softening phenomenon. This feature may be illustrated in Figure 3d in which the work hardening rate, defined as the slope of the stress-plastic strain curve, is plotted as a function of stress. Figure 3c presents the three network parameters as a function of temperature. The model constants in Eqs. (17), (18) and (20) were successively iterated in order to achieve optimal agreement between the model and the orientation hardening region on both sides of the glass transition. The thermal conductivity effect could have been taken into account as in (Guo et al., 2018b, 2018c) but only homogeneous simulations under isothermal conditions were considered.

Figure 5 shows the ability of the model to reproduce the main features of the stress-strain curves up to large-strains for the different compression temperatures and strain-rates. That indicates that the proposed approach provides a good approximation of the intrinsic elastoviscoplastic-viscohyperelastic response of this polymer and the basic underlying thermo-mechanical mechanisms. Quite interestingly, the model accounts for the abrupt change in intermolecular and network properties when the temperature traverses the glass transition temperature and the thermoplastic/rubber-like response transition. This point is fundamental in the aim reproducing the thermally-activated shape-memory effect.

3.3. Model prediction

The loading-unloading response, followed by cooling to T_0, freezes the macromolecular structure and the specimen shape by the appearance of an apparent plastic deformation comprising the viscoplastic intermolecular deformation and the network deformation not released after unloading. This frozen state is a non-equilibrium configuration for which the molecular network relaxation towards equilibrium is extremely long: an extremely long recovery time is needed as long as the temperature is held constant. Successive compressions are presented in Figure 6 for increasing compression temperatures (from 298 K to 393 K) and decreasing compression temperatures (from 393 K to 298 K). Each constant-temperature curve is followed by a cooling to T_0. The experiments were replicated by the model using the constants calibrated in Section 3.2 by considering two kinds of simulations under isothermal conditions: (i) in the first one, named intermittent simulations, the material is considered as a stress-free/strain-free medium at the beginning of each cycle, (ii) in the second one, named continuous simulations, the apparent plasticity at zero-stress is kept in memory for the next cycle. In other words, the continuous simulations consider the thermo-mechanical history seen by the material during the successive compressions. The internal intermolecular and network stresses are accumulated in different extents according to their dependence on the temperature and on the strain level reached. The results of the two kinds of simulations are presented in Figures 6 and 7, respectively, and, with no surprise, the model is found to describe in a better manner the response by considering continuous simulations. The agreement between simulations and experiments is very good when the compression temperature increases. When the compression temperature decreases, the accumulation of the network stress stored in the material provokes an overestimation of the response for the lowest temperature. Even if the strain level was small enough to avoid orientation hardening, the relative contribution of the network stress increases with temperature. Xia and Tian (2019) showed that the strain hardening behavior of pre-deformed amorphous polymers is more accurately captured using a dissipative dynamics of molecular network orientation than using a temperature-dependent hardening modulus. The difference observed in Figure 7b at room temperature is thus potentially due to the way (from the rheological point of view) that the temperature-dependent hardening modulus (characterizing the molecular network orientation process) interacts with the temperature-dependent viscosity of the strain-hardening (characterizing the molecular network relaxation process).

The thermally-activated strain recovery is related to an abrupt change in the ability of the polymer chain segments to rearrange towards equilibrium when the temperature traverses the glass transition. At a heating temperature of 433 K, Figure 8 provides the zero-stress creep response of polycarbonate specimens previously deformed at a strain of 70% and a temperature of 298 K. The recovery response is characterized by an initial rapid transient followed by the trend to reach a stabilization for which there is no significant strain change. It can be observed that the recovery response depends on the previous mechanical history in terms of strain-rate. The initial rapid transient and the equilibrium exhibit also a dependence on the heating temperature as shown in Figure 9. The experiments in Figures 8 and 9 were replicated by the model using the constants calibrated in Section 3.2. The simulations were performed by a compression at the glassy state (at 298 K) up to a strain of 70% followed by an unload until zero-stress. Then, while the zero-stress was maintained constant, the remaining of the simulation was a temperature jump to the glass transition followed by a progressive heating at a rate of 0.05 K s^{-1} until the holding temperature of heating. Figures 8 and 9 depict the ability of the model to predict the recovery response. It appears that the level of agreement between the predicted and measured recovery response depends on the previous applied strain-rate. However, the general trends provided by the model may be considered as relatively satisfactory. Interestingly, the model is able to capture the dependence of the response on thermo-mechanical history and recovery conditions. The equilibrium reached at

the end of the zero-stress creep response does not lead to a complete recovery of the apparent plasticity. This incomplete strain recovery is highly dependent on coupled effects of strain-rate and heating temperature and is reproduced by the model thanks to the consideration of the intrinsic strain-rate/temperature-dependent response coupled to the recovery-assisted network stress above T_g. Indeed, in our approach, viscoplastic intermolecular deformation and viscous network deformation are both strain-rate dependent and thermally-activated during the different steps of the loading-unloading-recovery process (Figure 4). The level of applied deformation is also an important condition of the mechanical history by accumulation of the two deformations. Its effect on the degree to which the strain is recovered is seen in the predictions provided in Figure 10. The model shows an important strain-rate dependency of the strain-level effect on the equilibrium state.

4. Concluding remarks

As concluding remarks, we have presented a physically-based model able to reproduce the elastoviscoplastic-viscohyperelastic response of amorphous thermoplastics in connection to the underlying thermo-mechanical mechanisms for below and above glass transition. The model successfully reproduced a series of experimental stress-strain data on polycarbonate and the abrupt change in response to a temperature variation over the entire range of strain-rates tested. The material kinetics with temperature was then used as inputs in the internal stress of network orientation/relaxation to drive the thermally-activated strain recovery process and the predictive capabilities of the model were verified under various conditions.

The generality endowed by the mathematical structure of the constitutive theory makes it applicable to the thermo-mechanical response of all amorphous thermoplastics and provides a useful tool to predict the thermally-induced strain recovery. In forthcoming works, MD simulations will be employed to better understand the deformation/recovery process in polymer systems in the final aim to propose enhanced continuum-based models.

Appendix A. Kinematics

The polymer medium is regarded as a homogeneous continuum body. As a basic quantity, the deformation gradient $\mathbf{F}=\partial \boldsymbol{x}/\partial \boldsymbol{X}$ maps a material point from its initial position $\boldsymbol{X}$ to the current position $\boldsymbol{x}$ once the body is loaded. The determinant of the deformation gradient $\mathbf{F}$ is noted $J=\det\left(\mathbf{F}\right)>0$ and its time derivative is $\dot{\mathbf{F}}=\mathbf{L}\mathbf{F}$ in which $\mathbf{L}=\partial \boldsymbol{v}/\partial \boldsymbol{x}$ is the spatial velocity gradient with $\boldsymbol{v}=\partial \boldsymbol{x}/\partial t$. The initial configuration of the continuum body is at a homogeneous absolute temperature θ_0 taken as reference and the current configuration is at a homogeneous absolute temperature θ different than θ_0. Using the conceptual sequence of configurations as proposed by Lee (1969) with the introduction of an intermediate stress-free thermal configuration at θ, the thermal deformation effects can be combined to the mechanical deformation of the continuum body and the deformation gradient $\mathbf{F}$ can take a multiplicative form. It is decomposed into a mechanical part $\mathbf{F}_M$ related to the isothermal stress-producing contribution and a thermal part $\mathbf{F}_\theta$ related to the stress-free thermal expansion of the continuum body:

$$\mathbf{F}=\mathbf{F}_M\mathbf{F}_\theta \tag{A1}$$

in which $\mathbf{F}_M=\partial \boldsymbol{x}/\partial \boldsymbol{X}_\theta$ and $\mathbf{F}_\theta=\partial \boldsymbol{X}_\theta/\partial \boldsymbol{X}$ are defined into the two successive arrangements, $\mathbf{X}_\theta$ being the position of the material point in the stress-free thermal configuration.

The determinant of the deformation gradient is $J=J_M J_\theta$ in which J_M and J_θ represent the intrinsic mechanical and thermal volume changes of the continuum body:

$$J_M = \det \mathbf{F}_M \text{ and } J_\theta = \det \mathbf{F}_\theta = \exp\left(\int_{\theta_0}^{\theta} 3\mu(u)\,du\right) \tag{A2}$$

where $\mu(\theta)$ is the temperature-dependent thermal expansion coefficient of the thermally isotropic continuum medium[8]; the thermal deformation gradient is $\mathbf{F}_\theta = J_\theta^{1/3}\mathbf{I}$ in which $\mathbf{I}$ is the identity tensor.

The spatial velocity gradient $\mathbf{L}$ is described by:

$$\mathbf{L} = \underbrace{\dot{\mathbf{F}}_M \mathbf{F}_M^{-1}}_{\mathbf{L}_M} + \underbrace{\mathbf{F}_M \dot{\mathbf{F}}_\theta \mathbf{F}_\theta^{-1} \mathbf{F}_M^{-1}}_{\mathbf{L}_\theta} \tag{A3}$$

in which $\mathbf{L}_M$ is the isothermal stress-producing part and $\mathbf{L}_\theta$ is the stress-free thermal part.

Due to the parallelism of the two resistances (see Figure 2), the intermolecular and network deformation gradients, $\mathbf{F}_I$ and $\mathbf{F}_N$, are both equal to the mechanical deformation gradient $\mathbf{F}_M$:

$$\mathbf{F}_M = \mathbf{F}_I = \mathbf{F}_N \tag{A4}$$

Considering an intermediate relaxed configuration at θ, the two deformation gradients, $\mathbf{F}_I$ and $\mathbf{F}_N$, can be in turn multiplicatively decomposed into elastic (or hyperelastic) and inelastic (viscoplastic or viscous) parts according to Lee decomposition:

$$\mathbf{F}_I = \mathbf{F}_I^{\mathrm{e}} \mathbf{F}_I^{\mathrm{vp}} \tag{A5}$$

$$\mathbf{F}_N = \mathbf{F}_N^{\mathrm{h}} \mathbf{F}_N^{\mathrm{v}} \tag{A6}$$

The different parts can be further decomposed into rotation $\mathbf{R}$ and stretching $\mathbf{U}$ or $\mathbf{V}$ (right or left, respectively) components:

$$\mathbf{F}_I^{\mathrm{e}} = \mathbf{R}_I^{\mathrm{e}} \mathbf{U}_I^{\mathrm{e}} = \mathbf{V}_I^{\mathrm{e}} \mathbf{R}_I^{\mathrm{e}} \text{ and } \mathbf{F}_I^{\mathrm{vp}} = \mathbf{R}_I^{\mathrm{vp}} \mathbf{U}_I^{\mathrm{vp}} = \mathbf{V}_I^{\mathrm{vp}} \mathbf{R}_I^{\mathrm{vp}} \tag{A7}$$

$$\mathbf{F}_N^{\mathrm{h}} = \mathbf{R}_N^{\mathrm{h}} \mathbf{U}_N^{\mathrm{h}} = \mathbf{V}_N^{\mathrm{h}} \mathbf{R}_N^{\mathrm{h}} \text{ and } \mathbf{F}_N^{\mathrm{v}} = \mathbf{R}_N^{\mathrm{v}} \mathbf{U}_N^{\mathrm{v}} = \mathbf{V}_N^{\mathrm{v}} \mathbf{R}_N^{\mathrm{v}} \tag{A8}$$

The intermolecular and network spatial velocity gradients, $\mathbf{L}_I$ and $\mathbf{L}_N$, are described by:

$$\mathbf{L}_I = \underbrace{\dot{\mathbf{F}}_I^{\mathrm{e}} \mathbf{F}_I^{\mathrm{e}^{-1}}}_{\mathbf{L}_I^{\mathrm{e}}} + \underbrace{\mathbf{F}_I^{\mathrm{e}} \dot{\mathbf{F}}_I^{\mathrm{vp}} \mathbf{F}_I^{\mathrm{vp}^{-1}} \mathbf{F}_I^{\mathrm{e}^{-1}}}_{\mathbf{L}_I^{\mathrm{vp}}} \tag{A9}$$

$$\mathbf{L}_N = \underbrace{\dot{\mathbf{F}}_N^{\mathrm{h}} \mathbf{F}_N^{\mathrm{h}^{-1}}}_{\mathbf{L}_N^{\mathrm{h}}} + \underbrace{\mathbf{F}_N^{\mathrm{h}} \dot{\mathbf{F}}_N^{\mathrm{v}} \mathbf{F}_N^{\mathrm{v}^{-1}} \mathbf{F}_N^{\mathrm{h}^{-1}}}_{\mathbf{L}_N^{\mathrm{v}}} \tag{A10}$$

The inelastic spatial velocity gradients, $\mathbf{L}_I^{\mathrm{vp}}$ and $\mathbf{L}_N^{\mathrm{v}}$, may be both decomposed as the sum of symmetric and skew-symmetric parts:

$$\mathbf{L}_I^{\mathrm{vp}} = \mathbf{F}_I^{\mathrm{e}} \dot{\mathbf{F}}_I^{\mathrm{vp}} \mathbf{F}_I^{\mathrm{vp}^{-1}} \mathbf{F}_I^{\mathrm{e}^{-1}} = \mathbf{D}_I^{\mathrm{vp}} + \mathbf{W}_I^{\mathrm{vp}} \tag{A11}$$

$$\mathbf{L}_N^{\mathrm{v}} = \mathbf{F}_N^{\mathrm{h}} \dot{\mathbf{F}}_N^{\mathrm{v}} \mathbf{F}_N^{\mathrm{v}^{-1}} \mathbf{F}_N^{\mathrm{h}^{-1}} = \mathbf{D}_N^{\mathrm{v}} + \mathbf{W}_N^{\mathrm{v}} \tag{A12}$$

in which $\mathbf{D}$ is the stretching rate tensor (symmetric part) and $\mathbf{W}$ is the spin tensor (skew-symmetric part):

$$\mathbf{D} = \frac{1}{2}\left(\mathbf{L} + \mathbf{L}^T\right) \text{ and } \mathbf{W} = \frac{1}{2}\left(\mathbf{L} - \mathbf{L}^T\right) \tag{A13}$$

It is assumed that the inelastic flow is volume preserving, i.e. $\det \mathbf{F}_I^{\mathrm{vp}} = 1$ and $\det \mathbf{F}_N^{\mathrm{v}} = 1$. Another convenient and frequently used hypothesis in the kinematics is irrotationality of the

[8] The thermal expansion coefficient, which may be deduced from the slope of the dilatation-temperature curve (Ovalle-Rodas et al., 2015), is $\mu(\theta)$ = 70.2 × 10^{-6} m/mK below the glass transition and $\mu(\theta)$ = 70.2 × 10^{-6} m/mK + 0.113/3T_g above the glass transition.

inelastic flow (Gurtin and Anand, 2005), i.e. $\mathbf{W}_I^{\mathrm{vp}} = \mathbf{0}$ and $\mathbf{W}_N^{\mathrm{v}} = \mathbf{0}$. The inelastic parts, $\mathbf{F}_I^{\mathrm{vp}}$ and $\mathbf{F}_N^{\mathrm{v}}$, of the intermolecular and network deformation gradients are then extracted from:

$$\dot{\mathbf{F}}_I^{\mathrm{vp}} = \mathbf{F}_I^{\mathrm{e}^{-1}} \mathbf{D}_I^{\mathrm{vp}} \mathbf{F}_I^{\mathrm{e}} \mathbf{F}_I^{\mathrm{vp}} \tag{A14}$$

$$\dot{\mathbf{F}}_N^{\mathrm{v}} = \mathbf{F}_N^{\mathrm{h}^{-1}} \mathbf{D}_N^{\mathrm{v}} \mathbf{F}_N^{\mathrm{h}} \mathbf{F}_N^{\mathrm{v}} \tag{A15}$$

Once the inelastic components, $\mathbf{F}_I^{\mathrm{vp}}$ and $\mathbf{F}_N^{\mathrm{v}}$, are computed, the elastic components, $\mathbf{F}_I^{\mathrm{e}}$ and $\mathbf{F}_N^{\mathrm{h}}$, are then extracted from Eqs. (A5) and (A6). The tensors $\mathbf{D}_I^{\mathrm{vp}}$ and $\mathbf{D}_N^{\mathrm{v}}$ defining the specificity of the model, with its strain-rate and temperature dependence, are constitutively outlined in the Subsection 2.2.

References

Ames, N.M., Srivastava, V., Chester, S.A., Anand, L., 2009. A thermo-mechanically coupled theory for large deformations of amorphous polymers. Part II: Applications. International Journal of Plasticity 25, 1495-1539.

Anand, L., Ames, N.M., Srivastava, V., Chester, S.A., 2009. A thermo-mechanically coupled theory for large deformations of amorphous polymers. Part I: Formulation. International Journal of Plasticity 25, 1474-1494.

Arruda, E.M., Boyce, M.C., 1993. A three-dimensional constitutive model for the large stretch behavior of rubber elastic materials. Journal of the Mechanics and Physics of Solids 41, 389-412.

Arruda, E.M., Boyce, M.C., Jayachandran, R., 1995. Effects of strain rate, temperature and thermomechanical coupling on the finite strain deformation of glassy polymers. Mechanics of Materials 19, 193-212.

Belbachir, S., Zaïri, F., Ayoub, G., Maschke, U., Naït-Abdelaziz, M., Gloaguen, J.M., Benguediab, M., Lefebvre, J.M., 2010. Modelling of photodegradation effect on elastic-viscoplastic behaviour of amorphous polylactic acid films. Journal of the Mechanics and Physics of Solids 58, 241-255.

Bergstrom, J.S, Boyce, M.C., 1998. Constitutive modeling of the large strain time-dependent behavior of elastomers. Journal of the Mechanics and Physics of Solids 46, 931-954.

Boatti, E., Scalet, G., Auricchio, F., 2016. A three-dimensional finite-strain phenomenological model for shape-memory polymers: Formulation, numerical simulations, and comparison with experimental data. International Journal of Plasticity 83, 153-177.

Bouaksa, F., Ovalle-Rodas, C., Zaïri, F., Stoclet, G., Naït-Abdelaziz, M., Gloaguen, J.M., Tamine, T., Lefebvre, J.M., 2014. Molecular chain orientation in polycarbonate during equal channel angular extrusion: Experiments and simulations. Computational Materials Science 85, 244-252.

Bouvard, J.L., Francis, D.K., Tschopp, M.A., Marin, E.B., Bammann, D.J., Horstemeyer, M.F., 2013. An internal state variable material model for predicting the time, thermomechanical, and stress state dependence of amorphous glassy polymers under large deformation. International Journal of Plasticity 42, 168-193.

Boyce, M.C., Parks, D.M., Argon, A.S., 1988. Large inelastic deformation of glassy polymers. Part I: Rate dependent constitutive model. Mechanics of Materials 7, 15-33.

Boyce, M.C., Socrate, S., Llana, P.G., 2000. Constitutive model for the finite deformation stress-strain behavior of poly(ethylene terephthalate) above the glass transition. Polymer 41, 2183-2201.

Buckley, C.P., Jones, D.C., 1995. Glass-rubber constitutive model for amorphous polymers near the glass transition. Polymer 36, 3301-3312.

Castro, F., Westbrook, K.K., Long, K.N., Shandas, R., Qi, H.J., 2010. Effects of thermal rates on the thermomechanical behaviors of amorphous shape memory polymers. Mechanics of Time-Dependent Materials 14, 219-241.

Chen, Y.C., Lagoudas, D.C., 2008a. A constitutive theory for shape memory polymers. Part I: Large deformations. Journal of Mechanics and Physics of Solids 56, 1752-1765.

Chen, Y.C., Lagoudas, D.C., 2008b. A constitutive theory for shape memory polymers. Part II: A linearized model for small deformations. Journal of Mechanics and Physics of Solids 56, 1766-1778.

Chen, X., Nguyen, T.D., 2011. Influence of thermoviscoelastic properties and loading conditions on the recovery performance of shape memory polymers. Mechanics of Materials 43, 127-138.

Dai, L., Tian, C., Xiao, R., 2020. Modeling the thermo-mechanical behavior and constrained recovery performance of cold-programmed amorphous shape-memory polymers. International Journal of Plasticity 127, 102654.

Diani, J., Liu, Y., Gall, K., 2006. Finite strain 3D thermoviscoelastic constitutive model for shape memory polymers. Polymer Engineering and Science 46, 486-492.

Doi, M., Edwards, M.F., 1986. The Theory of Polymer Dynamics. Oxford University Press, Oxford.

Ghosh, P., Srinivasa, A.R., 2013. A two-network thermomechanical model and parametric study of the response of shape memory polymers. Mechanics of Materials 60, 1-17.

Ghosh, P., Srinivasa, A.R., 2014. Development of a finite strain two-network model for shape memory polymers using QR decomposition. International Journal of Engineering Science 81, 177-191.

G'sell, C., Souami, A., 1997. Influence of crosslinking on the plastic behavior of amorphous polymers at large strains. Journal of Engineering Materials and Technology 119, 223-227.

Gudimetla, M.R., Doghri, I., 2017. A finite strain thermodynamically-based constitutive framework coupling viscoelasticity and viscoplasticity with application to glassy polymers. International Journal of Plasticity 98, 197-216.

Guo, Q., Zaïri, F., Guo, X., 2018a. Thermodynamics and mechanics of stretch-induced crystallization in rubbers. Physical Review E 97, 052501.

Guo, Q., Zaïri, F., Guo, X., 2018b. A thermo-viscoelastic-damage constitutive model for cyclically loaded rubbers. Part I: model formulation and numerical examples. International Journal of Plasticity 101, 106-124.

Guo, Q., Zaïri, F., Ovalle Rodas, C., Guo, X., 2018c. Constitutive modeling of the cyclic dissipation in thin and thick rubber specimens. Zeitschrift für Angewandte Mathematik und Mechanik 98, 1878-1899.

Guo, Q., Zaïri, F., Guo, X., 2018d. A thermo-viscoelastic-damage constitutive model for cyclically loaded rubbers. Part II: experimental studies and parameter identification. International Journal of Plasticity 101, 58-73.

Gurtin, M.E., Anand, L., 2005. The decomposition F= FeFp, material symmetry, and plastic irrotationality for solids that are isotropic-viscoplastic or amorphous. International Journal of Plasticity 21, 1686-1719.

Haward, R.N., Thackray, G., 1968. The use of a mathematical model to describe isothermal stress-strain curves in glassy thermoplastics. Proceedings of the Royal Society of London 302, 453-472.

Hu, J., Zhu, Y., Huang H., Lu, J., 2012. Recent advances in shape-memory polymers: Structure, mechanism, functionality, modeling and applications. Progress in Polymer Science 37, 1720-1763.

Lee, E. H., 1969. Elastic-plastic deformation at finite strains. Journal of Applied Mechanics 36, 1-6.

Lendlein, A., Kelch, S., 2002. Shape-memory polymers. Angewandte Chemie 41, 2034-2057.
Li, Y., He, Y., Liu, Z., 2017. A viscoelastic constitutive model for shape memory polymers based on multiplicative decompositions of the deformation gradient. International Journal of Plasticity 91, 300-317.
Lin, J.R., Chen, L.W., 1999. Shape-memorized crosslinked ester-type polyurethane and its mechanical viscoelastic model. Journal of Applied Polymer Science 73, 1305-1319.
Lion, A., 2000. Constitutive modelling in finite thermoviscoplasticity: A physical approach based on nonlinear rheological models. International Journal of Plasticity 16, 469-494.
Liu, Y., Gall, K., Dunn, M.L., Greenberg, A.R., Diani, J., 2006. Thermomechanics of shape memory polymers: Uniaxial experiments and constitutive modeling. International Journal of Plasticity 22, 279-313.
Mahjoubi, H, Zaïri, F., Tourki, Z., 2019. A micro-macro constitutive model for strain-inducedmolecularordering in biopolymers: Application to polylactide over a wide range of temperatures. International Journal of Plasticity 123, 38-55.
Mahjoubi, H, Zaïri, F., Tourki, Z., 2020. Strain-induced phase transformation in poly(lacticacid) across the glass transition: Constitutive model and identification. International Journal of Non-Linear Mechanics 118, 103241.
Mao, Y., Chen, F., Hou, S., Qi, J.H., Yu, K., 2019. A viscoelastic model for hydrothermally activated malleable covalent network polymer and its application in shape memory analysis. Journal of the Mechanics and Physics of Solids 127, 239-265.
Moon, S., Cui, F., Rao, I.J., 2019. A thermodynamic framework for the modeling of crystallizable triple shape memory polymers. International Journal of Engineering Science 134, 1-30.
Neki, K., Geil, P.H., 1973. Morphology-property studies of amorphous polycarbonate. Journal of Macromolecular Science, Part B: Physics 8, 295-341.
Nguyen, V.D., Lani, F., Pardoen, T., Morelle, X.P., Noels, L., 2016. A large strain hyperelastic viscoelastic-viscoplastic-damage constitutive model based on a multi-mechanism non-local damage continuum for amorphous glassy polymers. International Journal of Solids and Structures 96, 192-216.
Nguyen, T.D., Qi, H.J., Castro, F., Long, K.N., 2008. A thermoviscoelastic model for amorphous shape memory polymers: Incorporating structural and stress relaxation. Journal of the Mechanics and Physics of Solids 56, 2792-2814.
Ovalle-Rodas, C., Zaïri, F., Naït-Abdelaziz, M., Charrier, P., 2015. Temperature and filler effects on the relaxed response of filled rubbers: experimental observations on a carbon-filled SBR and constitutive modeling. International Journal of Solids and Structures 58, 309-321.
Park, H., Harrison, P., Guo, Z., Lee, M.G., Yu, W.R., 2016. Three-dimensional constitutive model for shape memory polymers using multiplicative decomposition of the deformation gradient and shape memory strains. Mechanics of Materials 93, 43-62.
Pyrz, M., Zaïri, F., 2007. Identification of viscoplastic parameters of phenomenological constitutive equations for polymers by deterministic and evolutionary approach. Modelling and Simulation in Materials Science and Engineering 15, 85-103.
Qi, H.J., Nguyen, T.D., Castro, F., Yakacki, C., Shandas, R., 2008. Finite deformation thermomechanical behavior of thermally-induced shape memory polymers. Journal of the Mechanics and Physics of Solids 56, 1730-1751.
Richeton, J., Ahzi, S., Daridon, L., Rémond, Y., 2005a. A formulation of the cooperative model for the yield stress of amorphous polymers for a wide range of strain rates and temperatures. Polymer 46, 6035-6043.

Richeton, J., Schlatter, G., Vecchio, K.S., Rémond, Y., Ahzi, S., 2005b. A unified model for stiffness modulus of amorphous polymers across transition temperatures and strain rates. Polymer, 46, 8194-8201.

Richeton, J., Ahzi, S., Vecchio, K.S., Jiang, F.C., Adharapurapu, R.R., 2006. Influence of temperature and strain rate on the mechanical behavior of three amorphous polymers: Characterization and modeling of the compressive yield stress. International Journal of Solids and Structures 43, 2318-2335.

Richeton, J., Ahzi, S., Vecchio, K.S., Jiang, F.C., Makradi, A., 2007. Modeling and validation of the large deformation inelastic response of amorphous polymers over a wide range of temperatures and strain rates. International Journal of Solids and Structures 44, 7938-7954.

Srivastava, V., Chester, S.A., Ames, N.M., Anand, L., 2010a. A thermo-mechanically-coupled large-deformation theory for amorphous polymers in a temperature range which spans their glass transition. International Journal of Plasticity 26, 1138-1182.

Srivastava, V., Chester, S.A., Anand, L., 2010b. Thermally actuated shape-memory polymers: Experiments, theory, and numerical simulations. Journal of the Mechanics and Physics of Solids 58, 1100-1124.

Su, X., Peng, X., 2018. A 3D finite strain viscoelastic constitutive model for thermally induced shape memory polymers based on energy decomposition. International Journal of Plasticity 110, 166-182.

Tervoort, T.A., Smit, R.J.M., Brekelmans, W.A.M., Govaert, L.E., 1997. A constitutive equation for the elasto-viscoplastic deformation of glassy polymers. Mechanics of Time-Dependent Materials 1, 269-291.

Tobushi, H., Hashimoto, T., Hayashi, S., Yamada, E., 1997. Thermomechanical constitutive modeling in shape memory polymer of polyurethane series. Journal of Intelligent Material Systems and Structures 8, 711-718.

Tobushi, H., Okumura, K., Hayashi, S., Ito, N., 2001. Thermomechanical constitutive model of shape memory polymer. Mechanics of Materials 33, 545-554.

Xiao, R., Tian, C., 2019. A constitutive model for strain hardening behavior of predeformed amorphous polymers: Incorporating dissipative dynamics of molecular orientation. Journal of the Mechanics and Physics of Solids 125, 472-487.

Yang, Q., Li, G., 2016. Temperature and rate dependent thermomechanical modeling of shape memory polymers with physics based phase evolution law. International Journal of Plasticity 80, 168-186.

Zaïri, F., Naït-Abdelaziz, M., Gloaguen, J.M., Lefebvre, J.M., 2010. Constitutive modelling of the large inelastic deformation behaviour of rubber-toughened poly(methyl methacrylate): Effects of strain rate, temperature and rubber-phase volume fraction. Modelling and Simulation in Materials Science and Engineering 18, 1-22.

Zaïri, F., Naït-Abdelaziz, M., Gloaguen, J.M., Lefebvre, J.M., 2011. A physically-based constitutive model for anisotropic damage in rubber-toughened glassy polymers during finite deformation. International Journal of Plasticity 27, 25-51.

Zhao, Q., Qi, H.J., Xie, T., 2015. Recent progress in shape memory polymer: New behavior, enabling materials, and mechanistic understanding. Progress in Polymer Science 49-50, 79-120.

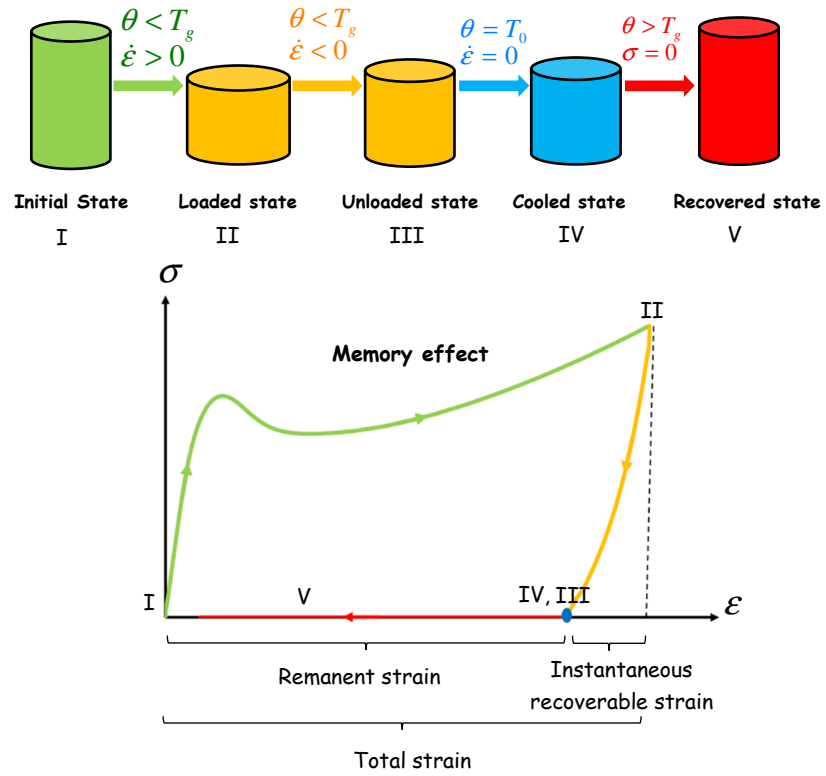

Figure 1. Thermally-induced shape-memory cycle of an amorphous polymer: deformation below T_g ($\mathrm{I} \rightarrow \mathrm{II}$: loading, $\mathrm{II} \rightarrow \mathrm{III}$: unloading), natural cooling at T_0 ($\mathrm{III} \rightarrow \mathrm{IV}$) and recovery of shape and remanent strain upon heating above T_g ($\mathrm{IV} \rightarrow \mathrm{V}$).

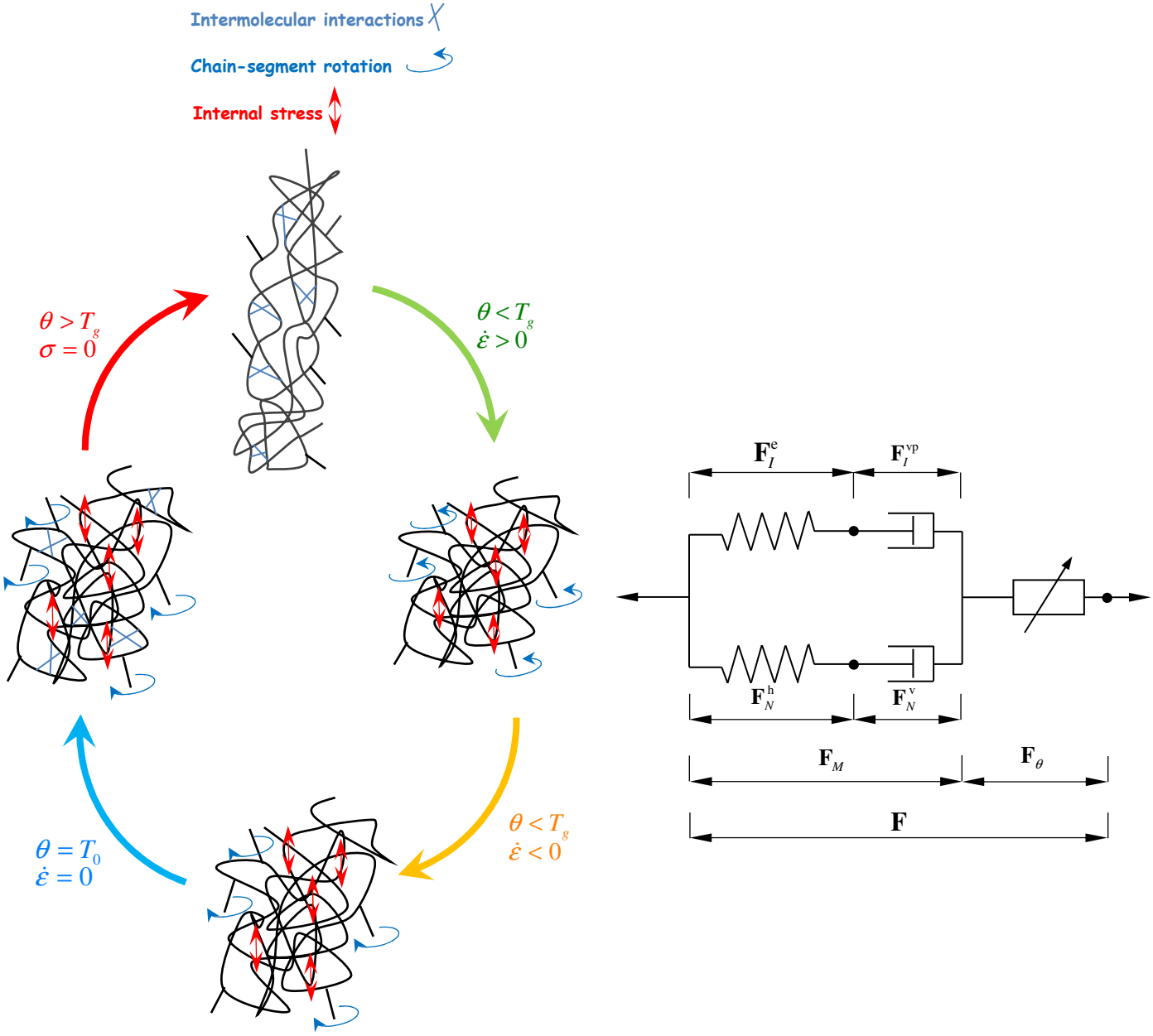

Figure 2. Molecular events in an amorphous network loaded in compression followed by the thermally-induced shape-memory cycle (the internal stress includes intermolecular and network stresses) and one-dimensional visualization of the model; the amorphous polymer deformation $\mathbf{F}$ is split into a thermal part $\mathbf{F}_\theta$ related to the stress-free thermal expansion and a mechanical part $\mathbf{F}_M$ related to the isothermal stress-producing contribution consisting in an elastoviscoplastic intermolecular branch in parallel with a viscohyperelastic network branch.

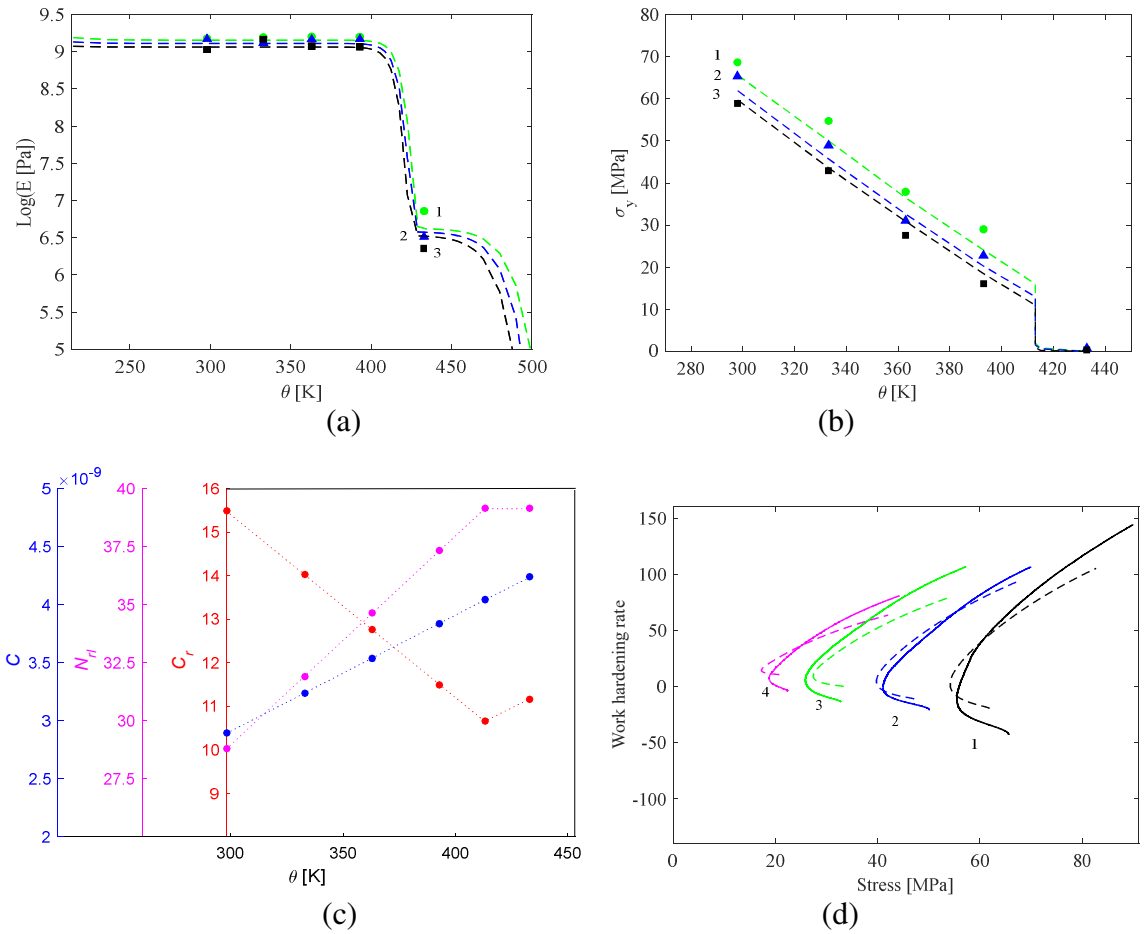

Figure 3. Intermolecular and network properties of polycarbonate as a function of temperature: (a) Young's modulus (1: 0.01 s^{-1}, 2: 0.001 s^{-1}, 3: 0.0001 s^{-1}), (b) yield stress (1: 0.01 s^{-1}, 2: 0.001 s^{-1}, 3: 0.0001 s^{-1}), (c) hardening modulus, average number of rigid links and viscosity constant, (d) work hardening rate-stress response at 0.001 s^{-1} (1: 298 K, 2: 333 K, 3: 363 K, 4: 393 K). The dashed lines represent the model and the symbols (the solid lines in (d)) represent the experiments.

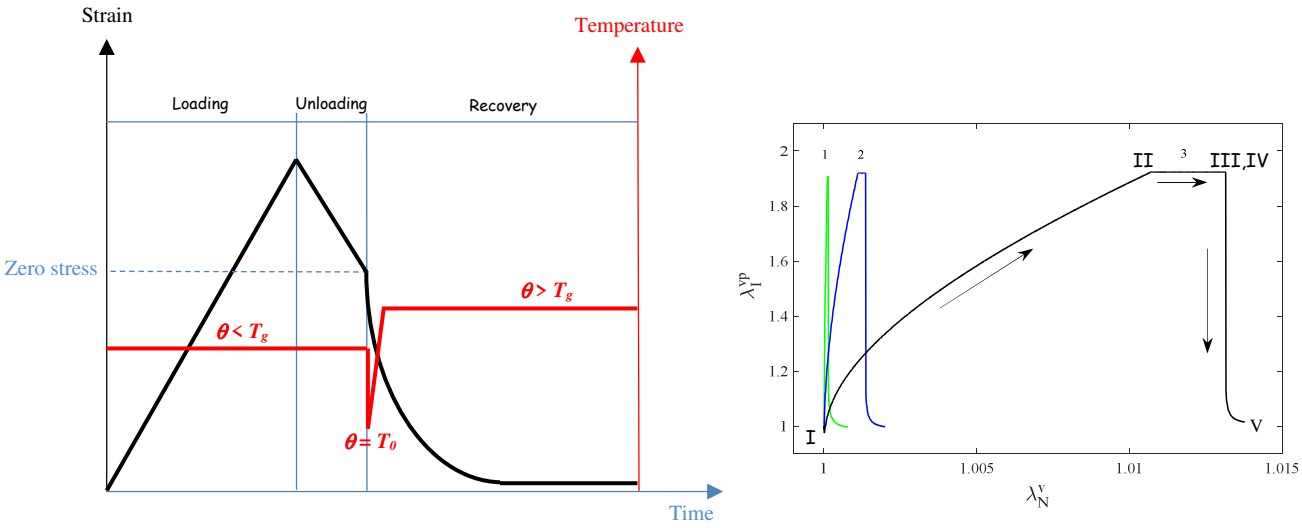

Figure 4. Loading-unloading-recovery process and corresponding viscoplastic intermolecular stretch as a function of viscous network stretch under different strain-rates, 1: 0.01 s^{-1}, 2: 0.001 s^{-1}, 3: 0.0001 s^{-1}, the steps $\mathrm{I} \rightarrow \mathrm{V}$ are those of Figure 1.

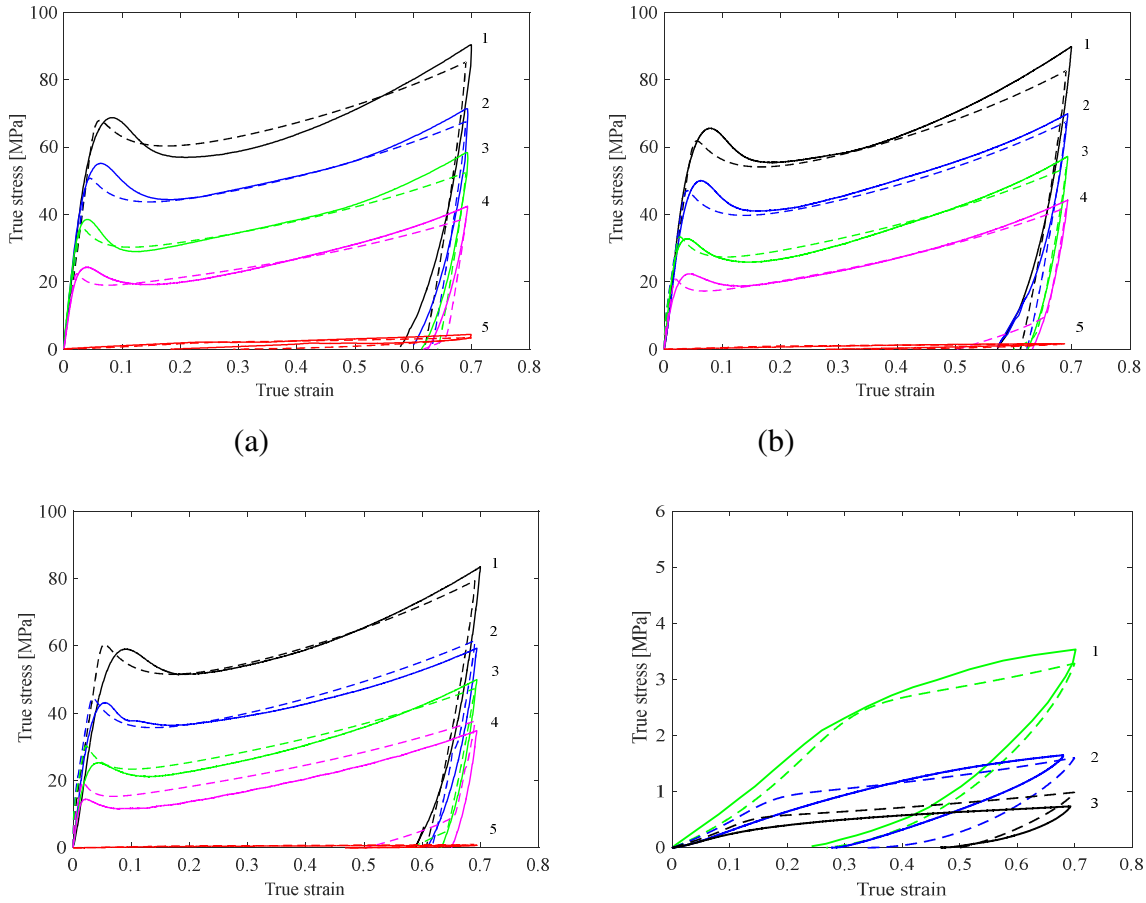

Figure 5. Model (dashed lines) vs. experiments (solid lines) of the stress-strain response of polycarbonate at different temperatures and strain-rates: (a) 0.01 s^{-1}, (b) 0.001 s^{-1}, (c) 0.0001 s^{-1}, 1: 298 K, 2: 333 K, 3: 363 K, 4: 393 K, 5: 433 K, (d) Zoom for 433 K, 1: 0.01 s^{-1}, 2: 0.001 s^{-1}, 3: 0.0001 s^{-1}.

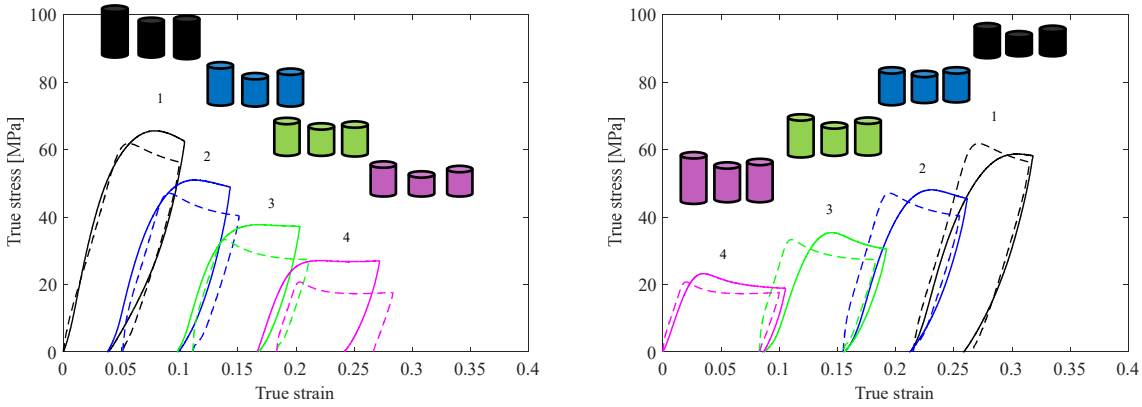

Figure 6. Model in intermittent (dashed lines) vs. experiments (solid lines) of the stress-strain response of polycarbonate successively deformed at a strain of 10% under different temperatures: (a) from 298 K to 393 K, (b) from 393 K to 298 K, 1: 298 K, 2: 333 K, 3: 363 K, 4: 393 K.

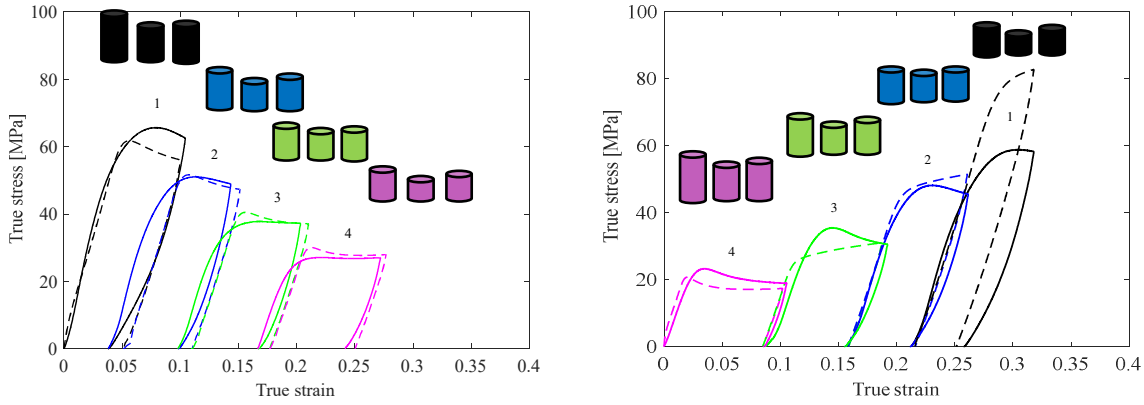

Figure 7. Model in continuous (dashed lines) vs. experiments (solid lines) of the stress-strain response of polycarbonate successively deformed at a strain of 10% under different temperatures: (a) from 298 K to 393 K, (b) from 393 K to 298 K, 1: 298 K, 2: 333 K, 3: 363 K, 4: 393 K.

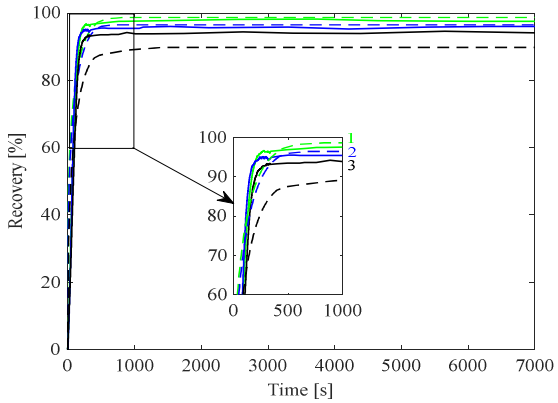

Figure 8. Model (dashed lines) vs. experiments (solid lines) of the zero-stress creep response at 433 K of polycarbonate specimens previously deformed at a strain of 70% and at 298 K under different strain-rates, 1: 0.01 s^{-1}, 2: 0.001 s^{-1}, 3: 0.0001 s^{-1}.

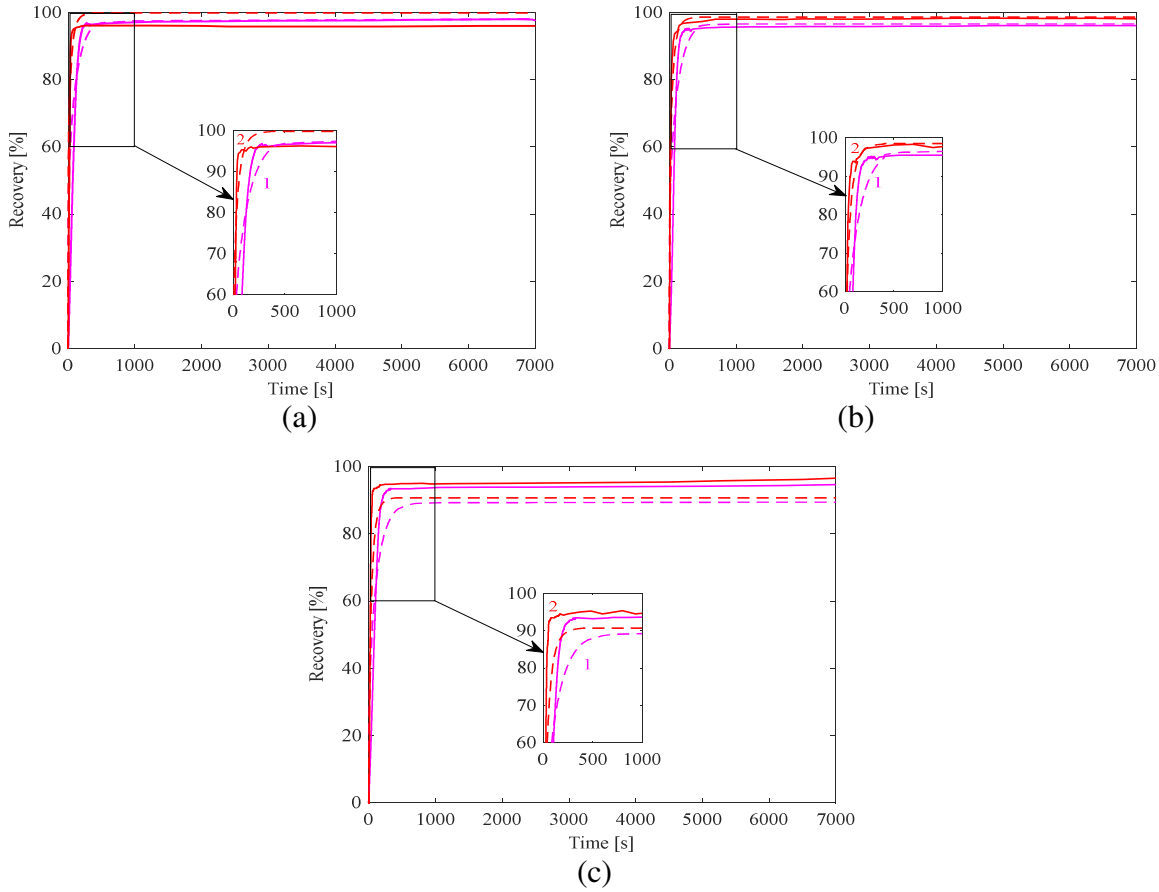

Figure 9. Model (dashed lines) vs. experiments (solid lines) of the zero-stress creep response at two different temperatures (1: 433 K, 2: 473 K) of polycarbonate specimens previously deformed at a strain of 70% and at 298 K under different strain-rates: (a) 0.01 s^{-1}, (b) 0.001 s^{-1}, (c) 0.0001 s^{-1}.

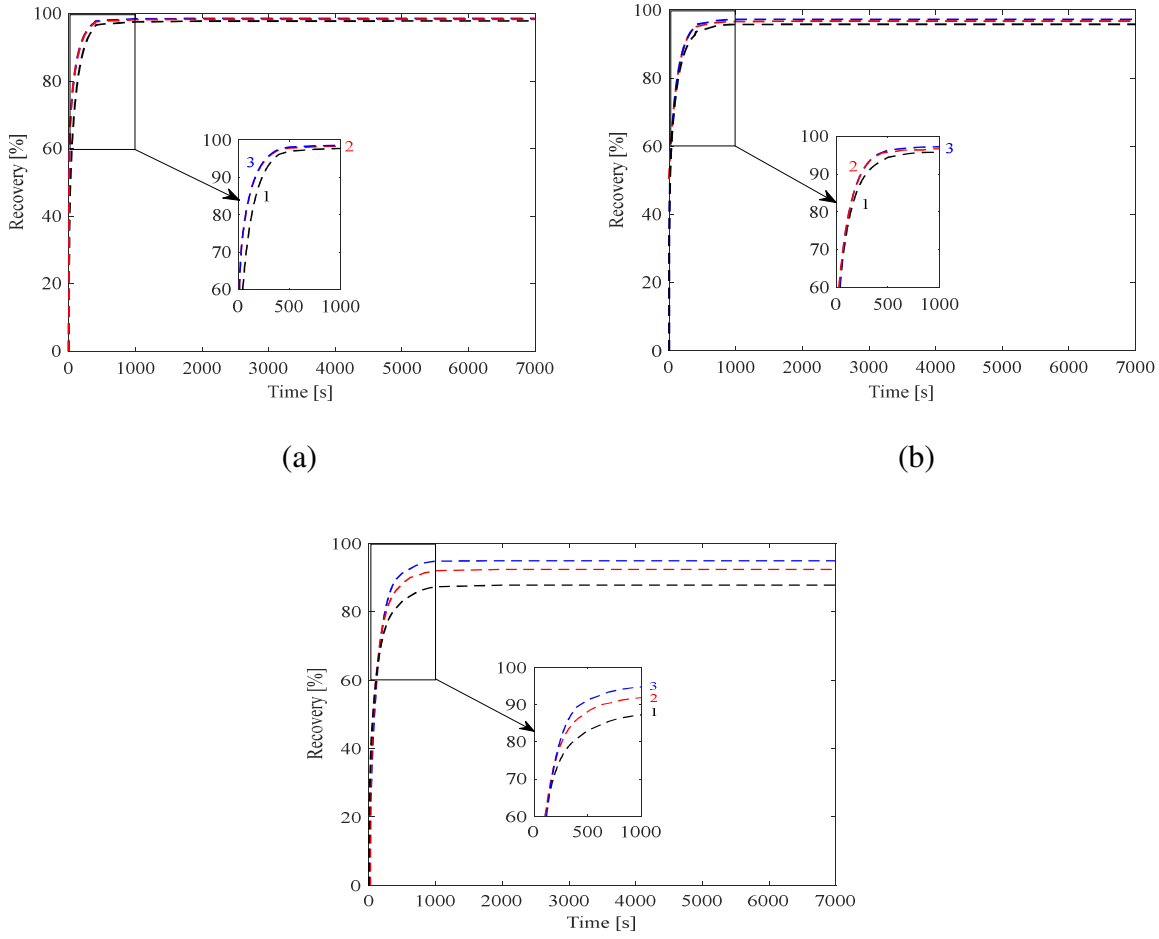

(a) (b)

(c)

Figure 10. Model predictions of the zero-stress creep response at 433 K of polycarbonate specimens previously deformed at different strains (1: 100%, 2: 70%, 3: 40%) and at 298 K under different strain-rates: (a) 0.01 s^{-1}, (b) 0.001 s^{-1}, (c) 0.0001 s^{-1}.

Parameter	Equation	Significance	Value
$T_{\beta ref}$ (K)	1	β transition temperature at $\dot{\varepsilon}_{ref}$	195
ΔH_β (J mol^{-1})	1, 27, 28	β activation energy	80×10^3
T_{gref} (K)	2	α transition temperature at $\dot{\varepsilon}_{ref}$	423
c_{1g}	2, 28	WLF coefficient	16.2
c_{2g} (K)	2, 28	WLF coefficient	55.6
T_{mref} (K)	3	Melting transition temperature at $\dot{\varepsilon}_{ref}$	493
m_1	5	Weibull shape parameter for β relaxation	5
m_2	6	Weibull shape parameter for α relaxation	80
m_3	7	Weibull shape parameter for melting	40
E_{1ref} (GPa)	8	Modulus at the beginning of β transition at $\dot{\varepsilon}_{ref}$	3.5
E_{2ref} (GPa)	9	Modulus at the beginning of α transition at $\dot{\varepsilon}_{ref}$	1.7
E_{3ref} (MPa)	10	Modulus at the beginning of melting at $\dot{\varepsilon}_{ref}$	5
s	8, 9, 10	Strain-rate sensitivity parameter of the stiffness modulus	0.08
$\sigma_{ps}/\sigma_{\mathrm{int}(t=0)}$	15	Ratio of intermolecular internal stresses	0.6
h (MPa)	15	Strain-softening slope	120
$\sigma_{\mathrm{int}(\theta=0)}$ (MPa)	16	Internal intermolecular stress at $\theta = 0$ K	59
m (MPa K^{-1})	16	Temperature sensitivity parameter of the internal intermolecular stress	0.133
α	16	Intermolecular mean stress sensitivity parameter	0.116
C_{r0} (MPa)	17, 18	Initial hardening modulus at $\theta = 0$ K	28
a (MPa K^{-1})	17, 18	Temperature sensitivity parameter of the initial hardening modulus	0.042
N_{rl0}	17, 18	Average number of rigid links at $\theta = 0$ K	1.96
b (K^{-1})	17, 18	Temperature sensitivity parameter of the average number of rigid links	0.09
C_0 (MPa^{-1} s^{-1})	20	Viscosity parameter at $\theta = 0$ K	-9.0×10^{-11}
c (MPa^{-1} s^{-1} K^{-1})	20	Temperature sensitivity parameter of the viscosity parameter	1.0×10^{-11}
$\dot{\gamma}_0$ (s^{-1})	27, 28	Pre-exponential factor	10.5×10^{16}
V (m^3)	27, 28	Activation volume	3×10^{-23}
n	27, 28	Parameter for the cooperative movement	5

Table 1. Model constants.

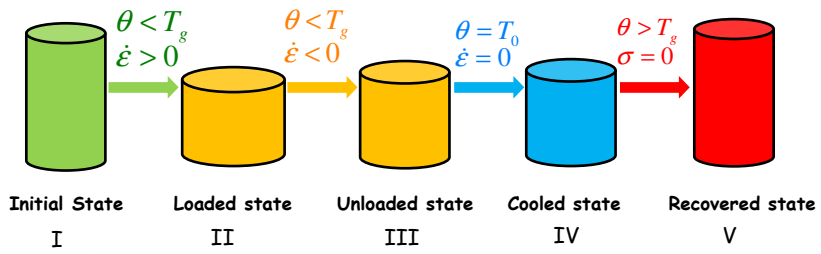
$\theta < T_g$
$\dot{\varepsilon} > 0$
$\theta < T_g$
$\dot{\varepsilon} < 0$
$\theta = T_0$
$\dot{\varepsilon} = 0$
$\theta > T_g$
$\sigma = 0$
Initial State
I
Loaded state
II
Unloaded state
III
Cooled state
IV
Recovered state
V

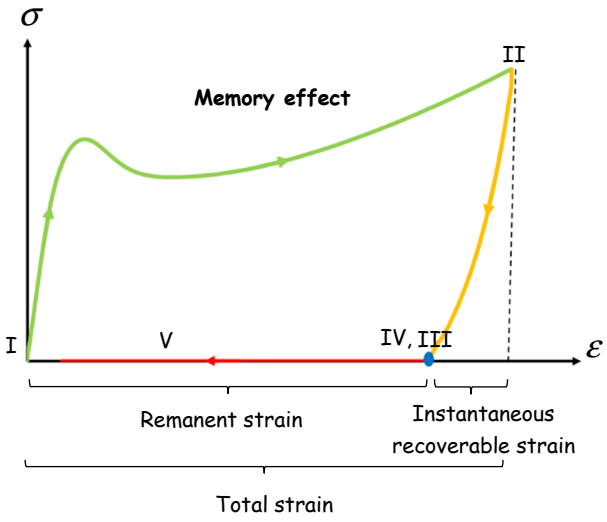
σ
II
Memory effect
I
V
IV, III
ε
Remanent strain
Instantaneous
recoverable strain
Total strain